2019

A Stress-Induced TRNA Depletion Response Mediates Codon-Based Translational Repression and Growth Suppression

Doowon Huh

A STRESS-INDUCED TRNA DEPLETION RESPONSE MEDIATES CODON-BASED TRANSLATIONAL REPRESSION AND GROWTH SUPPRESSION

A Thesis Presented to the Faculty of

The Rockefeller University

in Partial Fulfillment of the Requirements for

the degree of Doctor of Philosophy

by

Doowon Huh

June 2019

A STRESS-INDUCED TRNA DEPLETION RESPONSE MEDIATES CODON-BASED TRANSLATIONAL REPRESSION AND GROWTH SUPPRESSION

Doowon Huh, Ph.D.

The Rockefeller University 2019

Eukaryotic transfer RNAs (tRNAs) can become fragmented upon various cellular stresses, generating tRNA-derived RNA fragments (tRFs). Though this process has been observed for numerous cellular stresses and in many species ranging from plant cells to yeast and human cells, it is still poorly characterized and understood. Such tRNA fragmentation has previously been thought to affect a small fraction of the tRNA pool and was thus presumed to not affect the role of tRNAs in translation. We report that in human cells, oxidative stress can rapidly generate tRFs derived from tyrosyl $tRNA_{GUA}$—resulting in a significant depletion of the precursor tRNA molecule and mature tRNA while also leading to elevated levels of the tRF. Proteomic and ribosomal profiling of tyrosyl $tRNA_{GUA}$-depleted cells revealed impaired expression of proteins enriched in its cognate tyrosine codons, comprising growth and metabolic genes. Consistent with these affected pathways, depletion of tyrosyl $tRNA_{GUA}$ or its downstream targets, EPCAM, SCD, or USP3, repressed growth—revealing a tRNA-dependent growth suppressive pathway for oxidative stress response. A synthetic mimetic of the tRF induced upon oxidative stress was used to identify interactions with RNA binding

proteins through mass spectrometry. High-throughput sequencing of RNA isolated by crosslinking immunoprecipitation (HITS-CLIP) of hnRNPA1 and SSB confirmed the mass spectrometry results and identified endogenous reciprocal interactions between the protein and tRF. Binding of this tRF to hnRNPA1 inhibits destabilization of endogenous targets of this RNA binding protein, leading to increased mRNA expression of DNA damage response and cell cycle regulatory genes. Thus, tRNA fragmentation can both deplete a precursor tRNA molecule with codon-dependent regulatory consequences and also generate small-RNAs that can interact with and regulate RNA binding proteins.

Acknowledgements

I would first like to acknowledge my advisor, Sohail Tavazoie, for his mentorship and enthusiasm for science. He has fostered an environment where I could thrive as an independent thinker and has helped shape me into the scientist that I am today. I would also like thank my committee members, Dr. Charlie Rice, Dr. Paul Cohen, Dr. Olivier Elemento, and my external committee member Dr. Jeremy Wilusz. They have graciously offered their time and thoughts so that my research project could be as successful as possible. I am grateful to the Tri-I MD-PhD administrative office, especially Dr. Olaf Andersen, Dr. Jochen Buck, Dr. Catharine Boothroyd, and Dr. Ruthie Gotian. They have constructed an infrastructure that has allowed MD-PhD students to pursue a difficult undertaking with as much assistance as possible.

I would also like to thank all past and current members of the Tavazoie lab who have each contributed in their own way to my experience as a graduate student. I would especially like to acknowledge Dr. Hani Goodarzi who has helped with innumerable computational analyses for my project as well as providing instrumental feedback to my many questions over the years. I am grateful to all members of the lab who have helped with gathering experimental data including, Maria Passarelli, Jenny Gao, and Clara Goin. I would like to express my gratitude towards Lisa Noble, Chris Rouya, and Hoang Nguyen, all of whom have contributed not only to my scientific thinking but also to the overall enjoyment I have experienced in the lab.

I am thankful for my friends who have truly enriched my life outside of the lab and my family who have been incredibly understanding and supportive of my goals and aspirations. Most importantly, I would like to thank my wife, Sasha Benson. She has offered her unwavering encouragement and has given me strength whenever I have needed. I share all of my successes with her.

Table of Contents

List of Figures

Chapter 2

Chapter 3

List of Illustrations

Chapter 1

Chapter 5

List of Tables

Chapter 1

Chapter 3

Chapter 4

Materials and Methods

CHAPTER 1: Introduction

1.1 The biogenesis of and canonical roles for tRNAs

As a highly conserved class of noncoding RNA found in all three kingdoms of life, tRNAs are a product of Pol III transcription. After being transcribed, the pre-tRNA is then processed through numerous steps including, removal of the 5' leader and 3' trailer ends, splicing of introns, terminal 3' CCA addition, and modification of nucleoside residues, before a mature tRNA is exported to the cytoplasm (Phizicky and Hopper, 2010; Schimmel, 2018). In human cells, the nascent Pol III transcript is protected on the 3' end by SSB while RNase P is responsible for removal of the 5' leader sequence (Guerrier-Takada et al., 1983). Afterwards, the 3' trailer sequenced is trimmed by RNase Z (Maraia and Lamichhane, 2011). A small subset of tRNAs also contain introns, much like mRNAs, that must be removed before the maturation process is complete. Distinct from mRNAs however, tRNA introns are spliced through the tRNA splicing endonuclease (TSEN) complex (Peebles et al., 1979).

During this maturation process, certain nucleosides become modified with the average tRNA having 13 modifications (Pan, 2018). Many of the enzymes responsible for introducing these modifications have been identified in *S. cerevisiae*, though identifying the human orthologs are still a work in progress. Though all tRNA modifications have not been identified or their function known, modifications have been shown to improve tRNA stability, facilitate codon anticodon interactions for wobble base

pairing, prevent frameshifting, and other regulatory effects on the tRNA (Bjork et al., 1989; Helm et al., 1999; Kadaba et al., 2004; Konevega et al., 2004) (Table 1.1). Mature tRNAs have a conserved secondary structure that resembles a cloverleaf while the conserved tertiary structure resembles a tightly packed L-shaped structure.

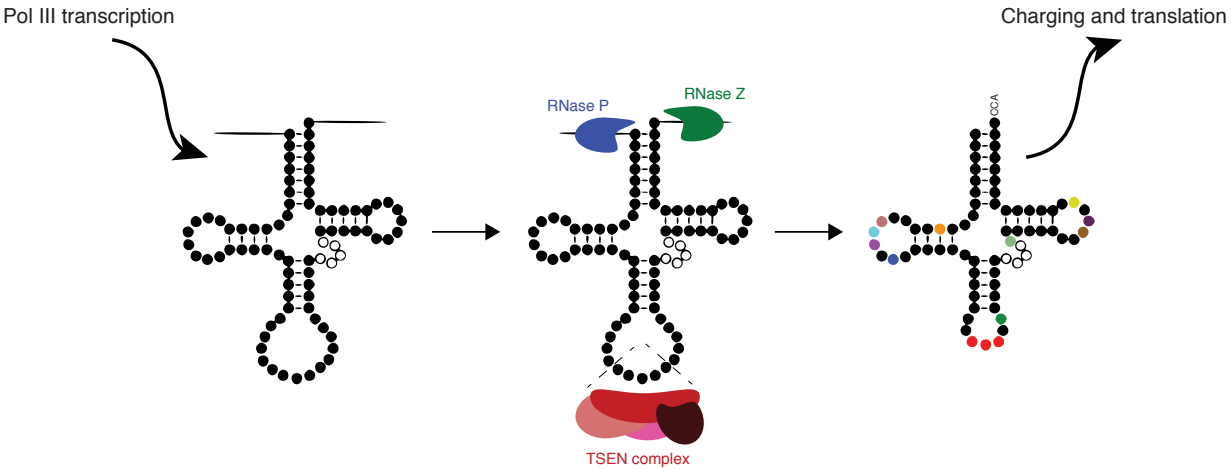

Illustration 1.1 A schematic of the maturation process for tRNAs.
After Pol III transcription, tRNAs require further processing before a mature and functional tRNA is able to take part in translation. The 5' leader and 3' trailer ends are removed as well as any introns found in the pre-tRNA. Terminal 3' CCA addition and modifications are added by many different enzymes before maturation is complete and the tRNA can be charged to take part in translation.

Before a mature tRNA is able to take part in its canonical role in decoding the genetic code, it must first be charged with its cognate amino acid. This ATP-

dependent reaction is catalyzed through a family of proteins known as the aminoacyl tRNA synthetases (aaRSs). In human cells, each tRNA has its own aaRS with the exception of the fusion protein EPRS, which charges both the glutamyl- and prolyl-tRNA (Cerini et al., 1991). Once the terminal 3' end is charged, this tRNA can now, in conjunction with the ribosome, take part in decoding the degenerate tri-nucleotide code (codons) of mRNAs to synthesize proteins.

Table 1.1. An example of modified nucleotides found in tRNAs.

Modification	Conventional abbreviation
Dihydrouridine	D
Inosine	I
Queuosine	Q
Pseudouridine	Ψ
Wybutosine	yW
1-methylguanosine	m^1G
1-methyladenosine	m^1A
1-methylinosine	m^1I
2-methylguanosine	m^2G
7-methylguanosine	m^7G
3-methylcytidine	m^3C
5-methylcytidine	m^5C
N^6-threonylcarbamoyladenosine	t^6A
N^2,N^2-dimethylguanosine	$m^{2,2}G$
5-methoxycarbonylmethyluridine	mcm^5U
5-methoxycarbonylmethyl-2-thiouridine	mcm^5s^2U
5-carbamoylmethyluridine	ncm^5U
5-taurinomethyluridine	tm^5U
5-taurinomethyl-2-thiouridine	tm^5s^2U

During translation, the ribosome has three internal sites where tRNAs can reside. Translation initiation occurs at the AUG start codon with an initiator $tRNA^{iMet}$ in the P-site of the ribosome. The A-site contains the next codon and is empty until the correct charged tRNA is present. The ability for a tRNA to read a specific codon is due to the Watson-Crick base pairing of the anticodon found in the anticodon loop of the tRNA. Once the proper charged tRNA enters the A-site, a peptidyl-transferase reaction creates a peptide bond between the growing polypeptide in the P-site with the newly incorporated amino acid in the A-site. The ribosome translocates by one codon resulting in the peptidyl-tRNA in the P-site and the now deacylated tRNA in the E-site, where it can exit the ribosome. This shift now creates a new and empty A-site where this cycle will continue until the termination codon is reached and the peptide is released as a newly synthesized protein.

The 20 amino acids are encoded by 61 different codons. The greater number of codons than amino acids necessitates multiple tRNAs encoding the same amino acid to read multiple different codons. Depending on the amino acid, there might exist anywhere from one to six different anticodons, which are termed isoacceptors. Furthermore, there also exist tRNAs that have the same anticodon but different body sequences of the tRNA, which are termed isodecoders. With the various permutations of isoacceptors and isodecoders, over 400 gene loci are found in the human genome that encode for tRNAs (Parisien et al., 2013). The number of loci that encode for a given isoacceptor can range from three to twenty-two.

Due to its importance in translation and the relatively long half-life of tRNAs, they are an abundant source of RNA in cells. As a group, tRNAs constitute 10-15% of the cell's total RNA. In comparison, ribosomal RNAs comprise ~80% of the cell's total RNA with the remaining population predominately being mRNAs.

1.2 New methods for measuring tRNA abundances

Given their high abundance found in all cell types, it was primarily thought that tRNAs were in excess to the amount necessary to sustain normal protein translation. Experimentally, it was challenging to test this notion as more commonly used reverse transcription-based methods used for mRNAs were ineffective for tRNAs. Due to the highly structured nature of tRNAs and the numerous modified bases that are found in the 76-90 nucleotide tRNA, they work poorly as substrates for reverse transcription. When confronted with a modified base, the reverse transcription enzyme has three outcomes. It can either read through the nucleotide correctly, insert an incorrect base-pair resulting in a mutation, or the enzyme can simply stall and fall off of the RNA completely. These truncated products are often too short to sequence and map to the genome with high confidence, leading to stochastic and inaccurate measurements of tRNA abundance. With the advent of high-throughput sequencing used to assess changes in mRNA abundances of ~20,000 genes in the transcriptome at once, it became even more apparent that the tRNA field was missing powerful tools to study the biology behind these important regulators of translation.

In 2006, the first paper to attempt to address tissue-specific tRNA expression was published using a microarray-based approach (Dittmar et al., 2006). This method circumvented the need to use reverse transcription as probe hybridization was the driving factor to detect abundance. As the first method to address this question with new experimental tools, it had a few caveats. The sensitivity and resolution of the method was relatively unknown as microarrays by nature have a lower dynamic range and the microarray chip only contained 42 probes for nuclear encoded tRNAs. Though these probes were designed to detect multiple tRNAs if sequence similarity was high, it fell short of addressing all 400+ loci and reduced resolution to the isoacceptor level, as opposed to the tRNA level. Moreover, as this microarray chip was not commercially available and difficult to synthesize, it was difficult for other labs to verify and follow up on these initial findings. Nonetheless, their efforts showed intriguing differences in levels of tRNAs in different human tissues and paved the way to experimentally test questions on the regulation of tRNAs.

Roughly 10 years after the tRNA microarray, multiple groups published methods on how to incorporate high-throughput sequencing methods with measuring tRNA abundances. Briefly summarized, these methods included various ways to bypass the effects of modified nucleosides on general reverse transcription through: (a) Treating tRNAs with AlkB, a demethylase, to reduce the number of modifications found on tRNAs (Cozen et al., 2015) (b) Using a novel reverse transcription enzyme that can read through modified bases at a higher rate, namely the thermostable group II intron reverse transcriptases (TGIRTs) (Zheng et al., 2015) (c) Fragmenting tRNAs through alkaline

hydrolysis so that smaller fragments become easier to sequence (Gogakos et al., 2017) (d) Using a probe-ligation based system to indirectly measure relative abundances of tRNAs (Goodarzi et al., 2016). The probe-ligation based method was used later in this thesis and will be explained in greater detail in Chapter 2.1. Each of these methods used to quantify tRNA has its own set of pros and cons, but they all pointed to the same conclusion – that tRNA expression was more complex than previously realized. Despite these new methods, development of tools to further quantify tRNAs to higher sensitivity and accuracy are still needed to fully explore the role tRNAs might have as a small non-coding RNA.

1.3 Increasing complexity in tRNA expression and function

With the idea that tRNA expression levels can now be measured with higher confidence, multiple studies recently have looked at the changes in tRNA abundance in the cell. The expression levels of some tRNAs were found to become modulated in the context of malignancy and cancer progression. Comparison of breast cancer cells to non-malignant breast cells revealed a number of tRNAs to be overexpressed and others repressed, perhaps owing to genomic instability and subsequent copy number alterations of different tRNA genes (Goodarzi et al., 2016; Pavon-Eternod et al., 2009). Such alterations in tRNA content were associated with altered cellular protein expression and mRNA stability. Studies of cancer progression revealed that upregulation of specific tRNA isodecoders through genomic copy number gains causally

enhanced expression of specific proteins that promoted cellular invasiveness and metastatic capacity. This study found that $tRNA^{Glu}_{UUC}$ and $tRNA^{Arg}_{CCG}$ were upregulated in highly metastatic cells, leading to an increased translation and protein expression of gene targets that contained complementary codons (Goodarzi et al., 2016). This study implicated novel proteins as mediators of breast cancer metastasis.

Another analysis revealed similar findings of large-scale tRNA expression alterations associated with the cancerous proliferative state versus the differentiated state. Proliferating cells had a tRNA pool different from differentiated/growth-arrested cells, leading to mRNA changes dependent on codon usage (Gingold et al., 2014). Mutagenesis studies of the *KRAS* oncogene also provided support for distinctness among 'synonymous' codons; KRAS protein expression became upregulated upon mutation of a 'rare' codon (decoded by a low-abundant tRNA isoacceptor) to an 'optimal' synonymous codon (decoded by an abundant tRNA isoacceptor) (Pershing et al., 2015) — consistent with tRNA availability impacting protein expression (Gustafsson et al., 2004). Low levels of certain tRNAs could result in decreased translational efficiency across the entire cell's proteomic landscape, but the inclusion of 'rare' or 'non-optimal' codons had negative effects on mRNA stability (Presnyak et al., 2015), potentially due to the aforementioned decreased translational efficiency.

If distinct isodecoders can modulate distinct sets of genes and yield distinct phenotypes, then one may expect the existence of a mutation in a tRNA isodecoder giving rise to a specific phenotype. Indeed, elegant genetic studies revealed that a mutation in the anticodon of a single nuclear encoded mouse tRNA gene could cause a

specific phenotype—cerebellar neurodegeneration (Ishimura et al., 2014). The combination of tRNA modification and abundance changes that can occur in the cell allow this non-coding RNA to have a widespread impact on gene and protein expression. As of now, we lack the mechanistic understanding of how tRNAs are regulated and the functional consequences but this offers the potential for a rich source of questions that future studies can dissect.

1.4 Discovery of tRNA derived fragments in response to stress

A recently discovered non-canonical role for tRNAs is that they can become fragmented as a source of small noncoding RNAs, termed tRNA-derived fragments (tRFs). As a highly abundant and conserved population of RNA, tRNAs are a prime candidate to act as molecules to respond immediately to changes in the cellular environment. Indeed, tRFs were first detected in response to starvation in *Tetrahymena* (Lee and Collins, 2005) and subsequently have been found to be induced by various stresses in yeast, plant, human, and many other model organisms (Thompson et al., 2008). A retrospective look reveals that tRFs might have been originally detected in urine from cancer patients (Gehrke et al., 1979). In response to stresses, tRNAs are thought to become fragmented on the timescale of minutes, markedly quicker than changes effected at the transcriptional level. Currently, a few ribonucleases have been implicated in generating tRFs in distinct species, including Rny1p in yeast and angiogenin (ANG) in human cells (Fu et al., 2009; Thompson and Parker, 2009a).

Rny1p has been found to be sequestered away in stress granules and released upon exposure to cellular stress (Fu et al., 2009; Thompson and Parker, 2009a). Given this low barrier and high abundance of tRNAs, it allows for a system that is quick, efficient, and can putatively react to specific stresses by identifying which tRNAs to cleave.

Rny1p and angiogenin are among the better characterized endonucleases that create tRNA halves, although there have been suggestions that other RNases such as Dicer may also create tRFs (Cole et al., 2009; Maute et al., 2013). High-throughput sequencing has identified many tRFs present in cells that represent the potential for many different tRNAs to give rise to one more tRFs each (Kumar et al., 2014). Future work will undoubtedly reveal other RNases cleave tRNAs and the context required for such an interaction.

Several groups have studied the effect of tRFs and the evidence suggests that tRFs may have wide ranging functions. In the context of cancer cells, it was previously shown that highly metastatic breast cancer cells blunted the induction of tRFs in response to hypoxia. In contrast, lowly metastatic breast cancer cells induced high levels of tRFs that would then bind to YBX1, an RNA-binding protein (RBP) that is commonly overexpressed in cancers. These tRFs, when bound to YBX1, would displace the RBP from its mRNA targets. Many mRNAs bound to YBX1 were known oncogenic promoters and once YBX1 was displaced, these mRNAs would decrease in stability and expression level. Thus, the induction of tRFs in this context acted as tumor suppressors by inhibiting the pro-metastatic effects of YBX1 and its effectors (Goodarzi et al., 2015).

Other studies have shown that certain tRFs can have the opposite effect of the YBX1-bound ones and promote tumorigenesis. One study found that in hormone-sensitive cancer cell lines, inhibition of angiogenin-mediated tRFs decreased cell growth (Honda et al., 2015). Similarly, another study found that inhibition of a 3' Leu^{CAG} tRF inhibited growth of hepatocellular carcinoma tumors and also promoted apoptosis. This 3' Leu^{CAG} tRF was found to bind directly to ribosomal protein mRNAs to improve their translation and the inhibition of the fragment led to a reduction in 40S ribosomal subunits (Kim et al., 2017). These differences in tRF effects demonstrate the possibility that specific fragments may have specific roles in cellular regulation.

Other gene regulatory roles for tRFs have also been identified in the context of epigenetic inheritance and hematopoiesis. Changes in diet of the male parent led to changes in tRFs in the mouse sperm cell that led to changes in gene expression in the zygote after fertilization (Chen et al., 2016; Sharma et al., 2016). Following a high fat diet, 5' tRFs from $tRNA^{Gly}_{CCC}$ in the sperm cells were able to repress genes regulated by the MERVL retrotransposon in the mouse embryo (Sharma et al., 2016). In hematopoiesis, ANG-mediated tRFs appeared to have contrasting phenotypes in hematopoietic stem/progenitor cells (HSPCs) compared to lineage-committed myeloid progenitor cells. In HSPCs, these tRFs acted to reduce protein synthesis and proliferation (Goncalves et al., 2016). The authors of this study hypothesized that this mechanism helped to maintain the stemness of HSPCs. In the myeloid progenitor cells however, the tRFs increased protein synthesis and cell proliferation.

Even though many roles for tRFs have been described by previous studies, it is still a vast underestimate of the potential regulatory role for these small noncoding RNAs. With the various isodecoders and isoacceptors available in each cell and the variety of cellular stresses in different tissue types, the network of potential regulation through tRFs will surely require further study.

CHAPTER 2: Identification and Validation of tRNAs and tRFs Modulated Upon Oxidative Stress

Although previous studies have shown that mature tRNA pools are dynamic and that they can be fragmented upon stress, it was thought that there was no link between the two. In response to stress, less than 5% of mature tRNAs were thought to be cleaved to produce tRFs (Saikia et al., 2012), suggesting that the mature tRNA pool would remain unchanged. This chapter will further explore this hypothesis and use high throughout sequencing to assess whether instances of mature tRNA reduction can be due to fragmentation during stress response. Using next-generation sequencing, we were able to measure changes between all different tRNA isoacceptors as well as tRFs in a bulk cell population following exposure to a given stress.

2.1 Evaluating tRNA abundances using tRNA profiling following oxidative stress

Due to the heavily modified nature of tRNAs, they are poor substrates for reverse transcription. To circumvent the problem of reverse transcribing tRNAs directly, a probe-ligation method was developed to indirectly measure relative differences (Goodarzi et al., 2016). This first step of this method required computationally deriving the fewest number of DNA probe pairs that could hybridize to the large number of isoacceptor and isodecoders present in the human genome. The probe pairs were designed so that hybridization to the tRNA would result in a single nucleotide gap between the 5' half and

3’ half. A DNA ligase would be used to fill in this nick, resulting in a DNA copy of the tRNA only when a 5’ and 3’ probe were present and hybridized to the tRNA. Isolation of the DNA copy and subsequent PCR amplification with the universal forward primer in the 5’ probe and a universal reverse primer in the 3’ probe allowed for high throughput sequencing of the complex set of tRNAs encoded by the human genome.

This tRNA profiling method was applied to RNA extracted from MCF10A cells, an immortalized human breast epithelial cell line, following 200uM hydrogen peroxide (H_2O_2) treatment at 8 and 24 hour time points after initial stress. H_2O_2 was chosen as it was previously shown to robustly induce tRFs (Thompson et al., 2008; Thompson and Parker, 2009a; Yamasaki et al., 2009). At both 8 and 24 hours after H_2O_2 treatment, tRNA levels were globally similar to the tRNA levels in the non-treated condition (Fig. 2.1). However, we noted that a number of specific tRNAs ($tRNA^{Tyr}_{GUA}$, $tRNA^{Ile}_{UAU}$, $tRNA^{Leu}_{UAA}$, $tRNA^{Thr}_{AGU}$, and others) significantly decreased in abundance, by linear regression analysis, over time after H_2O_2 treatment.

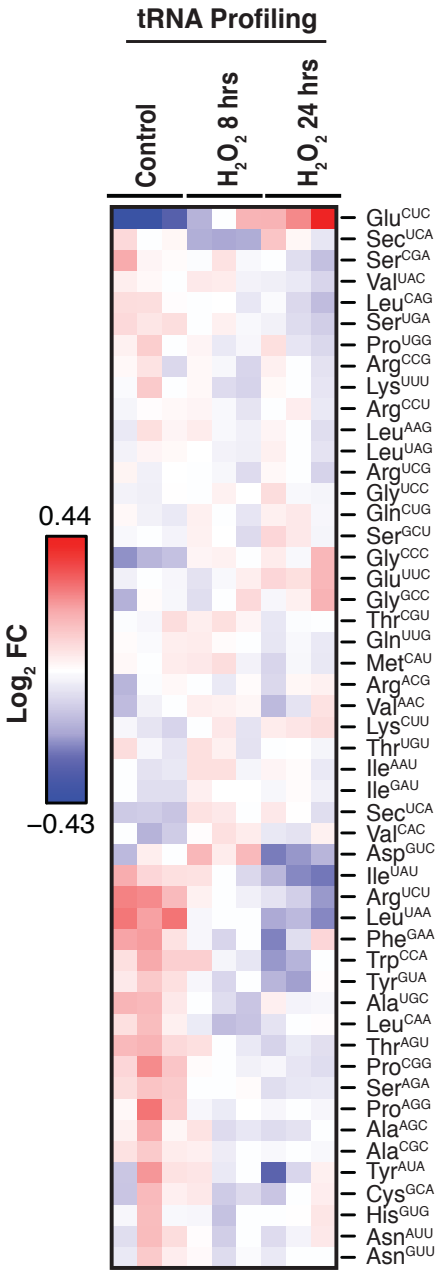

Figure 2.1. tRNA profiling of MCF10A cells after exposure to oxidative stress. Heatmap of tRNA profiling of MCF10A cells at 8 and 24 hours post exposure to oxidative stress (200μM H_2O_2). Biological triplicate data is depicted at each time point relative to control cells.

2.2 Identification and validation of tRF induction in MCF10A cells following oxidative stress

In order to test the hypothesis of if tRNA fragmentation could reduce mature tRNA levels, we sought to find the overlap between tRNAs that decreased and corresponding tRFs that increased with the same stress. Small RNA sequencing (smRNA-seq) was performed on RNA extracted from MCF10A cells exposed to H_2O_2. Consistent with previous studies, we noted numerous tRFs were induced upon oxidative stress (Fig 2.2A-B), with the highest induction found for tRF^{Tyr} and tRF^{Leu}.

A

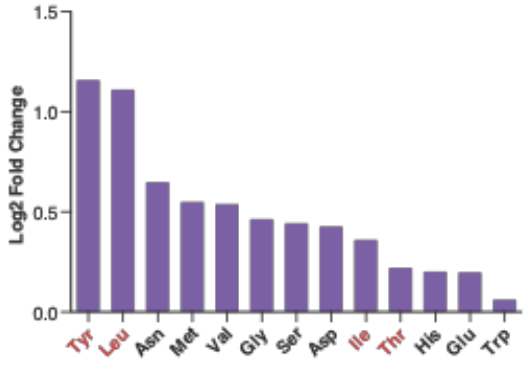

B

tRNA	Log_2 Fold change
Tyr^{GUA}	1.16
Leu^{CAA}	1.53
Leu^{TAA}	2.19
Leu^{CAG}	0.54
Leu^{AAG}	0.75
Leu^{TAG}	0.40
Ile^{TAT}	1.56
Ile^{AAT}	0.13
Thr^{TGT}	0.38
Thr^{AGT}	0.37

Figure 2.2. smRNA-seq of MCF10A cells for tRF induction. (A) MCF10A cells were exposed to oxidative stress (200μM H_2O_2) and processed for small RNA-sequencing. The log_2-fold induction levels for tRFs derived from distinct tRNA isoacceptor is plotted. (B) The log_2 fold induction of tRFs from smRNA-seq for all tRNAs that were significantly reduced in Fig 2.1.

Tyrosine and leucine were also found in the overlap between mature tRNAs that significantly were reduced upon oxidative stress and tRFs significantly induced by the same stress. Isoleucine and threonine were two other tRNAs that fit our criteria (Fig. 2.3). As tRF^{Tyr} and tRF^{Leu} exhibited the highest level of induction and therefore had the highest likelihood of affecting mature tRNA levels, further validation was performed for these two top hits.

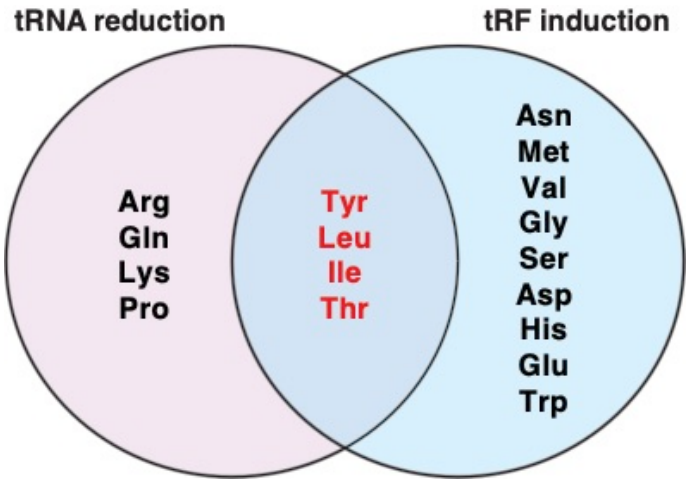

Figure 2.3. Overlap of tRNA and their derived fragments that changed upon oxidative stress. The overlap of tRNAs in that decreased over time with tRFs that were induced when MCF10A cells were exposed to oxidative stress. Four isoacceptor families of tRNAs are shown in the overlap with tyrosyl-tRNA and leucyl-tRNAs as the most promising candidates that exhibited the highest degree of tRF induction.

Northern blot validation confirmed the results of smRNA-seq and showed tRF induction for both tyrosyl-tRNA and leucyl-tRNAs (Fig 2.4A). However, a stronger and more robust induction was noted for tRF^{Tyr} and this conserved effect was seen in the nematode, *C. elegans*, after exposure to H_2O_2 (Fig 2.4B).

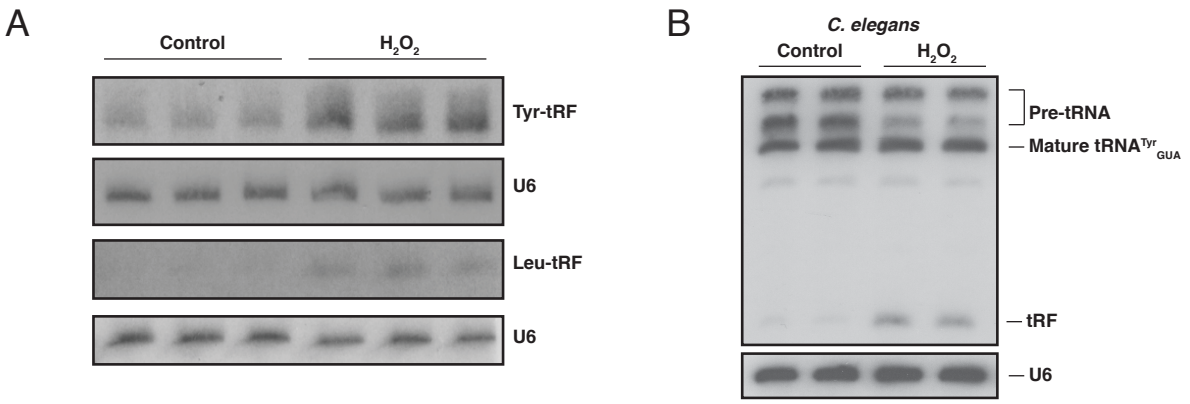

Figure 2.4. Northern blot validation of a tRF induction following oxidative stress.

(A) Northern blot for tRF^{Tyr}_{GUA} and tRF^{Leu}_{HAG} in MCF10A cells at one hour post oxidative stress (200µM H2O2) exposure. (B) Northern blot for tRF^{Tyr}_{GUA} in *C. elegans* cells at 15 minutes post oxidative stress (200µM H2O2) exposure.

2.3 Oxidative stress-induced fragmentation depletes tRNA$^{Tyr}_{GUA}$

A time course of the tRNA$^{Tyr}_{GUA}$ response to oxidative stress in MCF10A cells revealed multiple interesting findings. As previously shown, we noted an induction in the tRF$^{Tyr}_{GUA}$ following oxidative stress but surprisingly found that the tRF$^{Tyr}_{GUA}$ induction was rapid (within 5 minutes) was associated with a concomitant precipitous decline in pre-tRNA$^{Tyr}_{GUA}$ levels, which remarkably became nearly undetectable at 1-hour post treatment (Fig 2.5A-B). This suggests that, similar to the response in *C. elegans*, the majority of tRF$^{Tyr}_{GUA}$ is generated from the pre-tRNA$^{Tyr}_{GUA}$ rather than the mature tRNA. Pre-tRNA-derived tRFs have been previously detected in other contexts (Lee et al., 2009). As tRNAs are one of the most stable classes of RNAs, with relatively long half-lives, we would expect a delayed effect on the abundance of the mature tRNA pool upon acute reduction of the pre-tRNA pool. Indeed, we observed a significant delayed reduction in the tRNA$^{Tyr}_{GUA}$ pool, which was observed at 24 hours post H_2O_2 exposure (Fig 2.5A-B). The mature tRNA$^{Tyr}_{GUA}$ pool diminished to roughly half of pre-treatment levels at 24 hours post treatment. These observations reveal that oxidative stress-induced generation of tRF$^{Tyr}_{GUA}$ can significantly deplete the corresponding mature tRNA$^{Tyr}_{GUA}$ pool. Despite this reduction in mature tRNA$^{Tyr}_{GUA}$ levels following H_2O_2 exposure, other control tRNAs — tRNA$^{His}_{GUG}$ and tRNA$^{Glu}_{YUC}$ — remained unchanged relative to the control (Fig 2.6A-B). Our findings furthermore demonstrate that a single cellular stress can modulate the levels of a specific tRF and its corresponding tRNA.

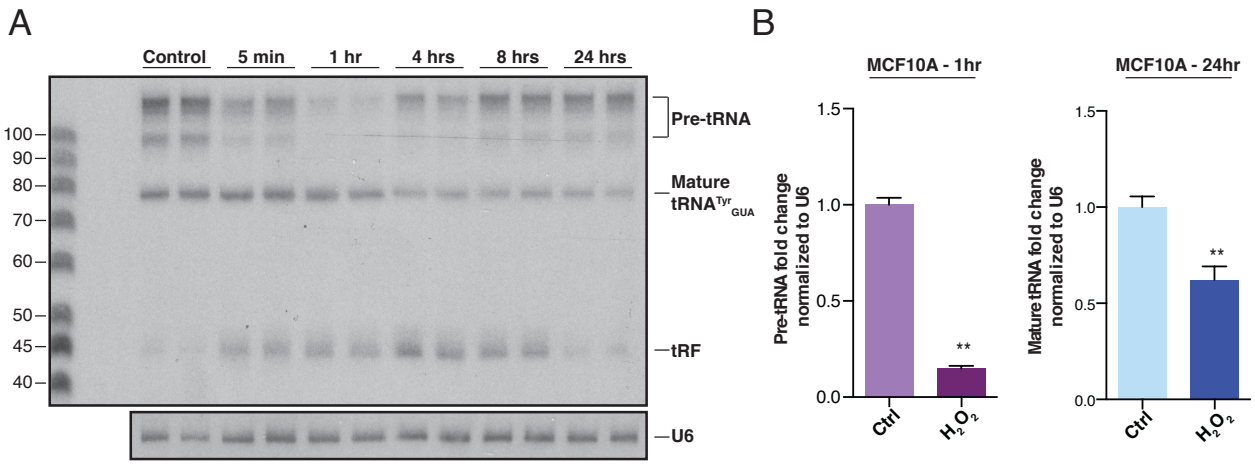

Figure 2.5. A time course for tRNA$^{Tyr}_{GUA}$ following oxidative stress.

(A) A northern blot depicting a time course experiment ranging from five minutes to 24 hours of MCF10A cells in response to oxidative stress. A single probe complementary to pre-tRNA$^{Tyr}_{GUA}$, mature tRNA$^{Tyr}_{GUA}$, and tRF$^{Tyr}_{GUA}$ expression was ^{32}P-labeled and used for detection. (B) Quantification of pre-tRNA$^{Tyr}_{GUA}$ northern blot analysis from multiple independent experiments after one hour as well as mature tRNA$^{Tyr}_{GUA}$ levels after 24 hours (normalized to U6 levels) are shown (n=6).

Data represent mean ± s.e.m.

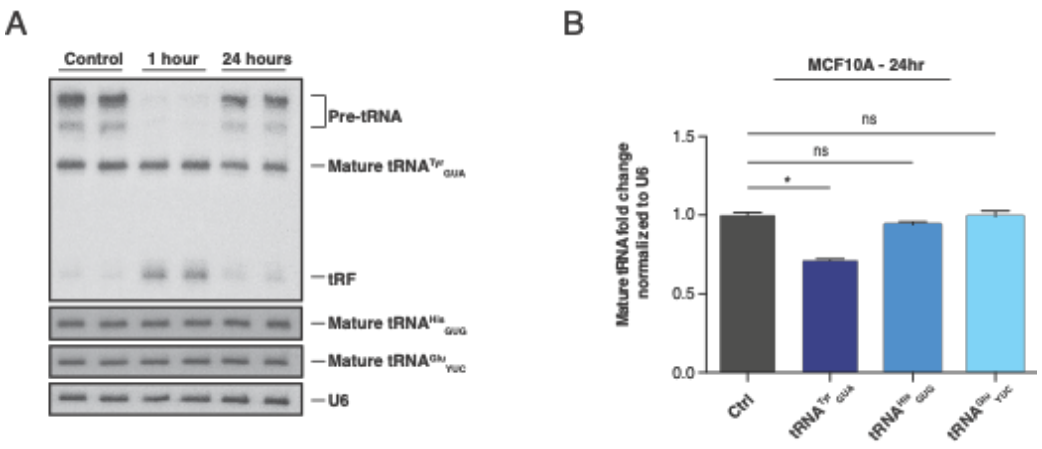

Figure 2.6. Reduction of other tRNAs are not seen with oxidative stress. (A) A northern blot depicting two time points, one hour and 24 hours, after exposure to oxidative stress (200μM H_2O_2) in MCF10A cells. As before, a single probe complementary to pre-tRNA$^{Tyr}_{GUA}$, mature tRNA$^{Tyr}_{GUA}$, and tRF$^{Tyr}_{GUA}$ was while another probe complementary to either the mature tRNA$^{His}_{GUG}$ or mature tRNA$^{Glu}_{YUC}$ were both ^{32}P-labeled and used for detection. (B) Quantification of tRNA$^{Tyr}_{GUA}$, tRNA$^{His}_{GUG}$, and tRNA$^{Glu}_{YUC}$ by northern blot analysis from two independent experiments 24 hours (normalized to U6 levels) after exposure to oxidative stress (200μM H_2O_2) are shown (n=4). A one-tailed Mann-Whitney test (*$p < 0.05$) was used to test for statistical significance between the treated and control cell lines for each time point. Data represent mean ± s.e.m.

We next determined whether oxidative stress-induced tRNA$^{Tyr}_{GUA}$ depletion is a transient response or whether it could persist upon continual exposure to stress. Exposure of cells to H_2O_2 once daily for five consecutive days maintained tRNA$^{Tyr}_{GUA}$ repression as assessed by northern blot analysis (Fig 2.7A-B). RNA was collected on the sixth day, 24 hours after the last H_2O_2 exposure and as before, tRF$^{Tyr}_{GUA}$ induction

was maintained over this time (Fig 2.7A-B). Such continuous H_2O_2 treatment repressed mature $tRNA^{Tyr}_{GUA}$ levels by roughly half. Similar to previous experiments, this effect appeared to be relatively specific to $tRNA^{Tyr}_{GUA}$ as $tRNA^{His}_{GUG}$ and $tRNA^{Glu}_{YUC}$ remained unchanged again.

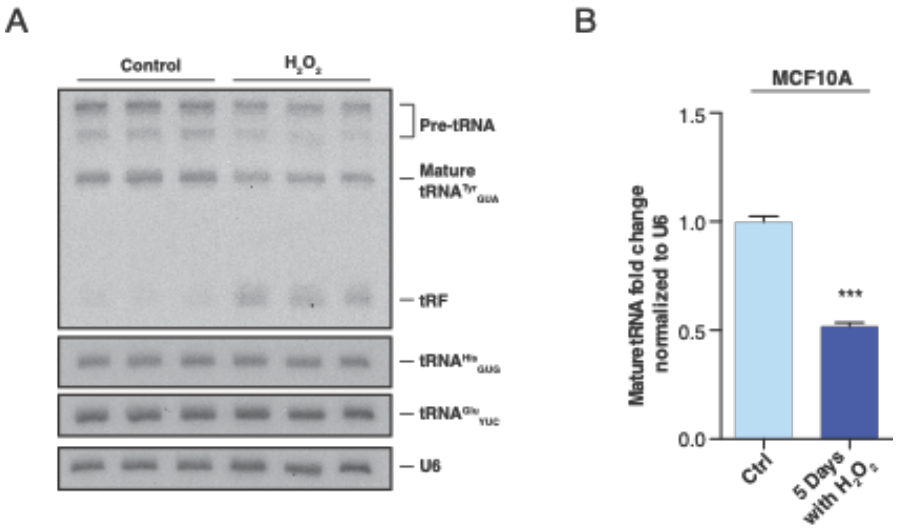

Figure 2.7. A repeated exposure to oxidative stress maintains a reduced level of $tRNA^{Tyr}_{GUA}$

(A) MCF10A cells were exposed to oxidative stress (200μM H_2O_2) once daily for five continuous days to test if repeated exposure to the stress could elicit a response similar to that found in a shorter time course. (B) Quantification of mature $tRNA^{Tyr}_{GUA}$ bands by northern blot after cells were treated once daily for five continuous days (normalized to U6) from multiple independent experiments (n=12).

Data represent mean ± s.e.m.

Similar responses to oxidative stress were seen when another cell line, HBEC30, was exposed to the same conditions. The HBEC30 cell line is an immortalized bronchial epithelial cell line that, similar to the MCF10A, showed an immediate pre-tRNA reduction and tRF induction in response to H_2O_2. A delayed reduction in the mature $tRNA^{Tyr}_{GUA}$ was also observed suggesting that these effects could represent a cellular response seen in many different cell types and organisms (Fig 2.8A-B).

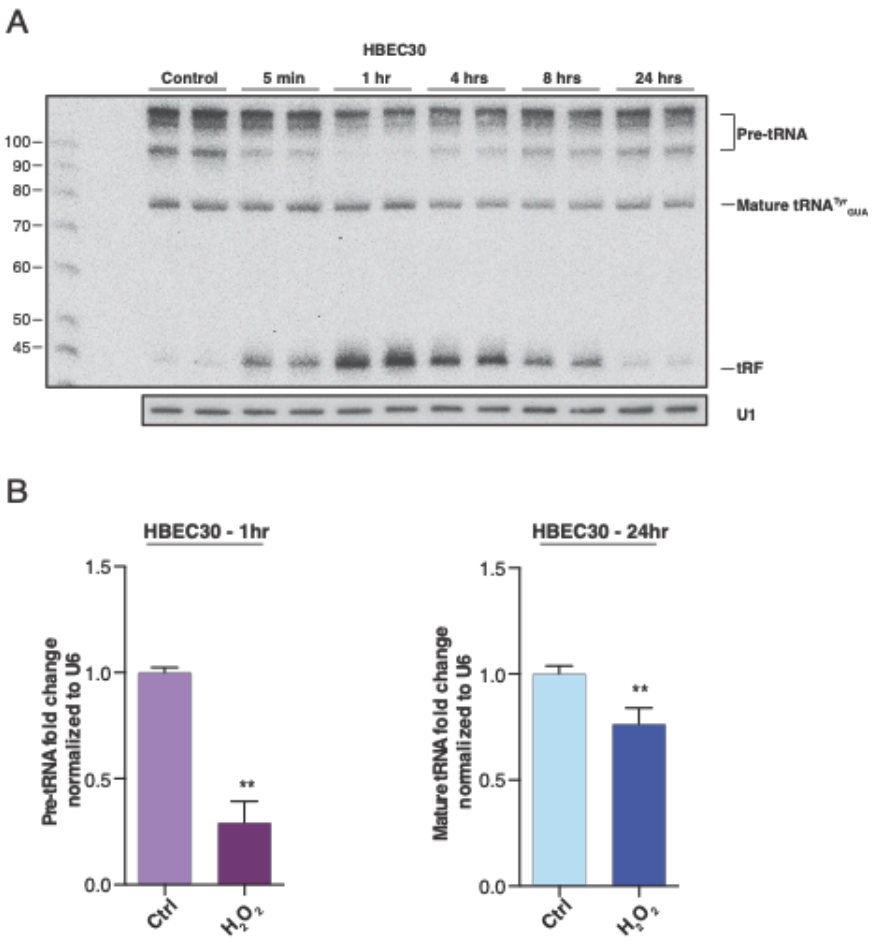

Figure 2.8. Similar responses to oxidative stress are observed in HBEC30 cells

(A) A northern blot depicting a time course experiment ranging from five minutes to 24 hours for HBEC30 cells in response to oxidative stress (200μM H_2O_2). As before, a single probe complementary to pre-tRNA$^{Tyr}_{GUA}$, mature tRNA$^{Tyr}_{GUA}$, and tRF$^{Tyr}_{GUA}$ was ^{32}P-labeled and used for detection. (B) Quantification of northern blot analysis for pre-tRNA$^{Tyr}_{GUA}$ (left) and tRNA$^{Tyr}_{GUA}$ (right) after one hour and 24 hours respectively in HBEC30 cells upon exposure to oxidative stress (200μM H_2O_2) as before (n=6). Data represent mean ± s.e.m.

To further confirm that $tRNA^{Tyr}_{GUA}$ levels are dependent on exposure to oxidative stress, we used an independent source of oxidative stress. Menadione, a commonly used pharmacological agent to induce oxidative stress, yielded similar results to that of H_2O_2. A reduction of the pre-tRNA and induction of the tRF was noted at shorter time points while mature $tRNA^{Tyr}_{GUA}$ levels are significantly reduced by 24 hours (Fig 2.9A-B).

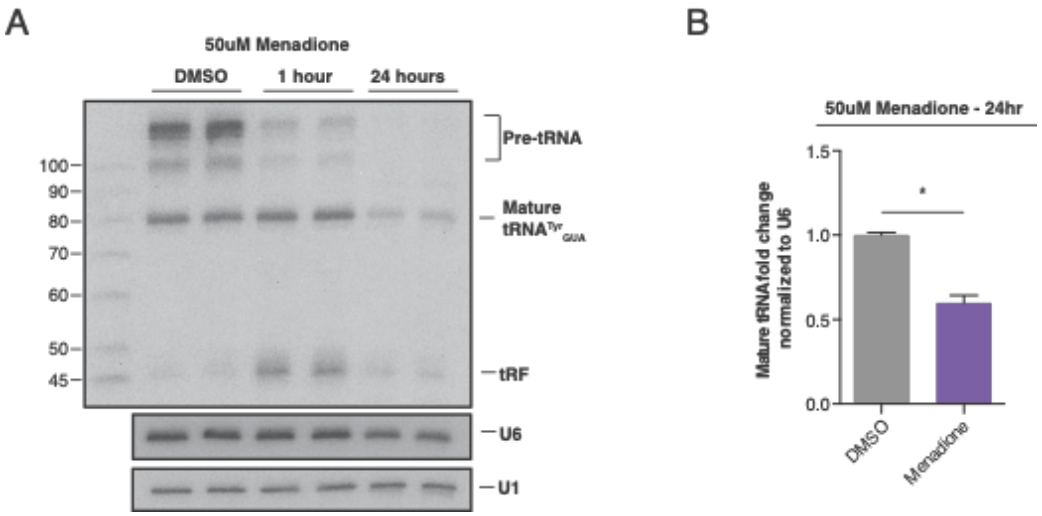

Figure 2.9. A secondary source of oxidative stress elicits the same response from MCF10A cells

(A) A northern blot at a shorter and longer time point after MCF10A cells were treated with a pharmacological agent used to induce oxidative stress (menadione). (B) Quantification of $tRNA^{Tyr}_{GUA}$ by northern blot analysis from two independent experiments 24 hours (normalized to U6 levels) after exposure to oxidative stress (50μM menadione) are shown (n=4). A one-tailed Mann-Whitney test (*$p < 0.05$) was used to test for statistical significance.

Data represent mean ± s.e.m.

2.4 Oxidative stress-induced fragmentation is not due to cell death

Given the rapid and extensive fragmentation of the pre-tRNA$^{Tyr}_{GUA}$, the possibility remained that this effect was due to RNA degradation during cellular death. However, the experimental data showed that the observed induction of tRFs was not an artifact of cell death, as cell viability was unchanged in treated versus control samples at the concentration of H_2O_2 used (Fig 2.10A). Consistent with previous data of tRNA$^{His}_{GUG}$ and tRNA$^{Glu}_{YUC}$ being unchanged in the context of oxidative stress, no global RNA degradation was observed even 24 hours after oxidative stress exposure (Fig 2.10B). Our findings argue against the likelihood of a tRF$^{Tyr}_{GUA}$ induction and tRNA$^{Tyr}_{GUA}$ reduction due to cell death. Instead, it appears that this tRNA is selectively cleaved upon oxidative stress in a dynamic process.

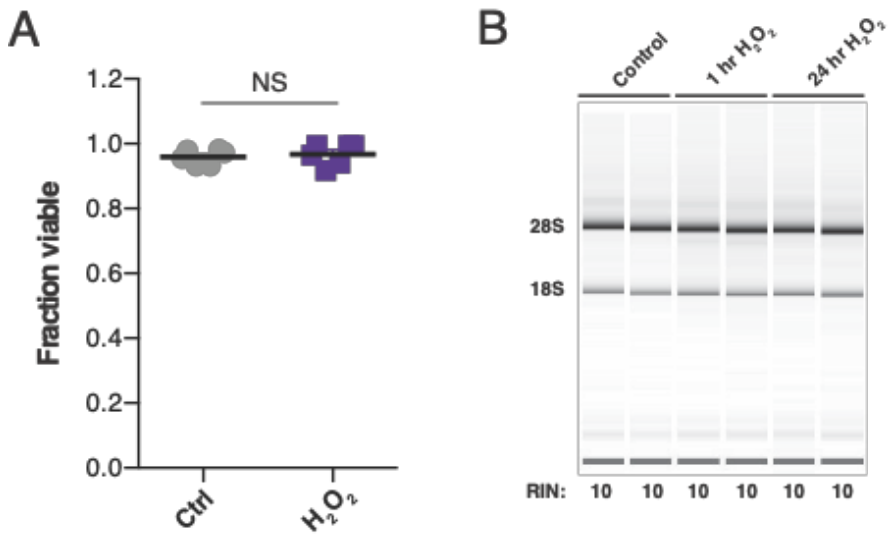

Figure 2.10. Fragmentation upon oxidative stress is not due to cell death

(A) The viability of MCF10A cells after H_2O_2 treatment (200μM) was tested by a trypan blue exclusion assay (n=6). Viability was tested one hour after exposure to oxidative stress. A two-tailed Mann-Whitney test was used to test for statistical significance between the treated and control cell lines for each time point. (B) RNA extracted from cells exposed to oxidative stress for one hour or 24 hours were analyzed for RNA integrity.

Data represent mean ± s.e.m.

2.5 Summary

In this chapter, we identify that a specific pre-tRNA is cleaved in response to oxidative stress. This fragmentation response has two downstream effects. The first being that a tRF^{Tyr}_{GUA} is immediately induced while the second effect is that the mature $tRNA^{Tyr}_{GUA}$ is reduced in a more delayed response. This finding is contrary to previous thoughts that tRNA fragmentation occurs in such low levels for a given tRNA that the mature tRNA pool remains relative unaffected. This fragmentation effect is seen in different cell lines and species but is not secondary to cell death. The effects of a tRF^{Tyr}_{GUA} induction and a $tRNA^{Tyr}_{GUA}$ will be the focus of the next two chapters.

CHAPTER 3: Molecular and Cellular effects of $tRNA^{Tyr}_{GUA}$ Depletion

As an abundant class of RNA with longer half-lives, it was thought that tRNAs were in excess and not a limiting factor in translation. With the degenerate nucleotide sequence leading to different codons encoding the same amino acid, these synonymous codons were thought to be relatively identical. However, recent studies have offered new perspectives to show that tRNAs might be regulated and regulate more than previously expected.

One new perspective of tRNAs demonstrated that this class of noncoding RNA, similar to many other RNAs, were a dynamic population. Proliferating cells had a different population of tRNAs from differentiated or growth-arrested cells (Gingold et al., 2014) and that changes in tRNA abundance could lead to unique cellular phenotypes, such as increased metastatic capability (Goodarzi et al., 2016). These modulated tRNAs were able to exert their influence not only at the translational level, but also at the mRNA transcript level. Synonymous codons were not actually synonymous as some isoacceptors for a given amino acid were rarer, or non-optimal, compared to other isoacceptors. These non-optimal codons could result in lower levels of translational and mRNA degradation by greater dissociation from ribosomes (Presnyak et al., 2015).

This chapter will further explore the molecular and cellular effects of oxidative stress-induced $tRNA^{Tyr}_{GUA}$ depletion. By combining tools in molecular biology, computational biology, and cell assays, we were able to assess changes on the global and single gene level that were downstream of $tRNA^{Tyr}_{GUA}$ depletion.

3.1 Orthogonal approaches to deplete $tRNA^{Tyr}_{GUA}$

In general, tRNAs are stable compared to other RNA species and often have multiple genetic loci that encode each tRNA. For $tRNA^{Tyr}_{GUA}$, 11-12 genetic loci are thought to encode for $tRNA^{Tyr}_{GUA}$, where each loci has high conservation of sequence for the mature exons between them. The introns for each loci vary in both sequence and length. Utilizing this high sequence conservation between all loci, two initial approaches were designed to reduce $tRNA^{Tyr}_{GUA}$ levels.

The first method employed using CRISPRi to target as many genetic loci at once and inhibit transcription of the tRNA through the use of a catalytically null Cas9 (dCas9) mutant. CRISPR itself was avoided as the high number of loci meant that the cell would experience a high number of double-stranded breaks of the cutting by Cas9 was efficient or the cell would retain enough loci to keep levels of the tRNA high if the cutting was inefficient. Guide RNAs (sgRNA) were designed to target up to 12 loci at once for CRISPRi to reduce levels of $tRNA^{Tyr}_{GUA}$. However, after selection for cells stably expressing dCas9 and the sgRNA, northern blot revealed that CRISPRi had little effect on mature $tRNA^{Tyr}_{GUA}$ levels (Fig 3.1).

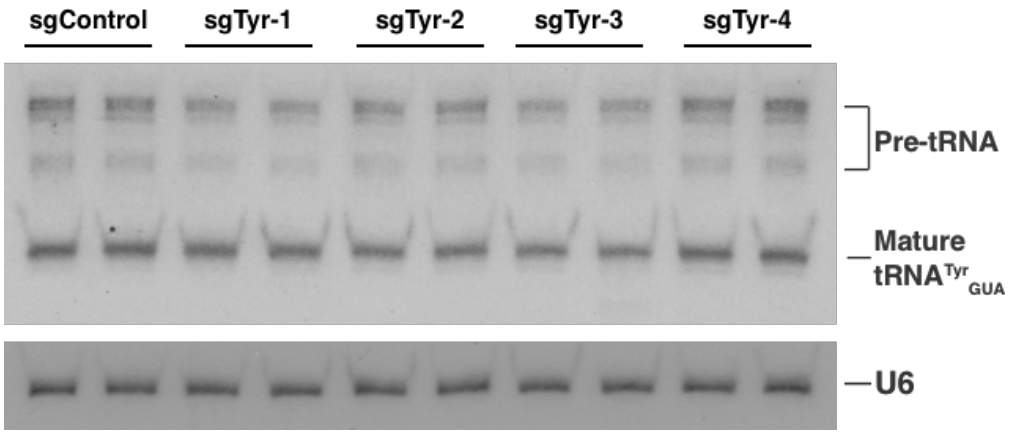

Figure 3.1. CRISPRi was ineffective at reducing levels of tRNA$^{Tyr}_{GUA}$
There was no difference in tRNA$^{Tyr}_{GUA}$ levels after expressing sgRNAs and dCas9 designed to target up to 12 tRNA$^{Tyr}_{GUA}$ genomic loci at the same time.

The high sequence similarity between all tRNA$^{Tyr}_{GUA}$ was also targeted using short-hairpin RNAs (shRNA). RNAi against the tRNA itself resulted in a roughly 50% reduction in levels of the tRNA by northern blot analysis (Fig 3.2A). This reduction was remarkably similar to the reduction seen by oxidative stress and may represent the greatest amount of tRNA$^{Tyr}_{GUA}$ depletion allowed for cells to remain viable. Due to the small size of the tRNA itself however, multiple different shRNAs could not be identified effectively reduce tRNA$^{Tyr}_{GUA}$ levels. As an independent loss-of-function approach, we sought to impair cellular utilization of tRNA$^{Tyr}_{GUA}$ via RNAi-mediated depletion of its cognate amino acid charging enzyme—the tyrosyl-tRNA synthetase (YARS) gene (Fig

3.2B-C) We reasoned that depletion of aminoacylated $tRNA^{Tyr}_{GUA}$ caused by YARS knockdown would phenocopy $tRNA^{Tyr}_{GUA}$ depletion as in both cases, $tRNA^{Tyr}_{GUA}$–mediated tyrosine incorporation into proteins is impaired.

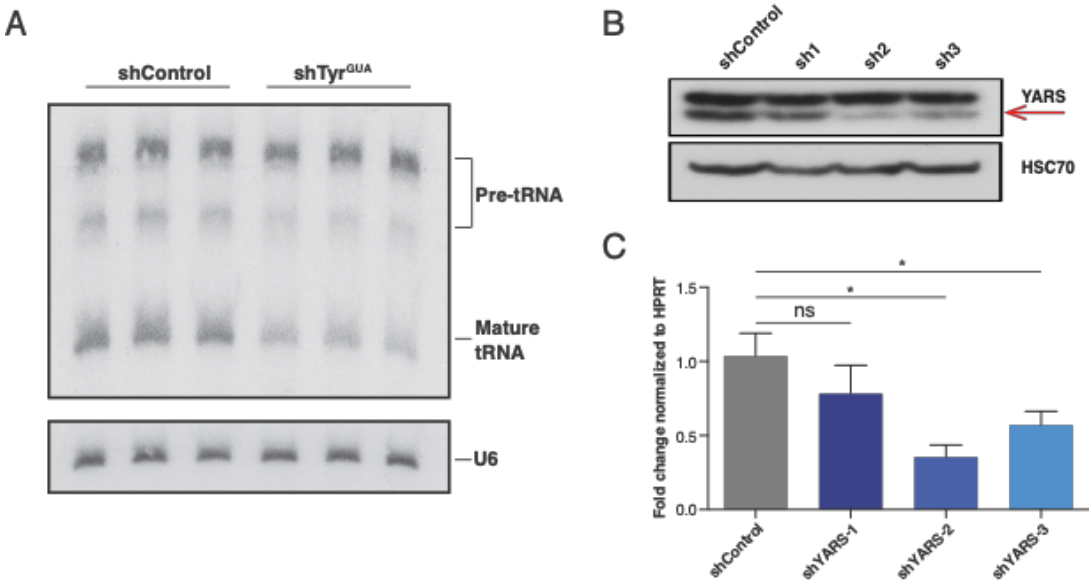

Figure 3.2. Orthogonal methods of depleting functional levels of $tRNA^{Tyr}_{GUA}$

(A) Northern blot of MCF10A cells expressing a control short-hairpin RNA or a hairpin targeting $tRNA^{Tyr}_{GUA}$. (B) A western blot of MCF10A expressing a control short-hairpin RNA or a hairpin targeting the tyrosyl-tRNA synthetase, YARS (red arrow). HSC70 was used as a loading control. (C) Total mRNA from MCF10A cells stably expressing a short hairpin targeting YARS was analyzed by quantitative RT-PCR. The two cell lines with the best knockdown were used for subsequent experiments. A one-tailed Mann-Whitney test ($*p < 0.05$) was used to test for statistical significance between the treated and control cell lines for each time point.

Data represent mean ± s.e.m.

When using RNAi to target the tRNA itself, these shRNA would be specific for $tRNA^{Tyr}_{GUA}$. However, two codons, UAC and UAU, encode for the tyrosine amino acid. RNAi against YARS would presumably prevent charging of both $tRNA^{Tyr}_{GUA}$ and $tRNA^{Tyr}_{AUA}$. Upon northern blot analysis, we were unable to detect $tRNA^{Tyr}_{AUA}$. Due to guanine-uracil wobble base pairing (Crick, 1966; Ladner et al., 1975; Quigley and Rich, 1976), $tRNA^{Tyr}_{GUA}$ can recognize both codons (UAC and UAU) that code for the amino acid tyrosine. This suggested that $tRNA^{Tyr}_{AUA}$ might represent a very rare isoacceptor, if expressed at all, and may play a minimal, if any, role in translation. This notion is consistent with what has been reported by others in additional mammalian cell types (dos Reis et al., 2004).

3.2 Oxidative stress-induced $tRNA^{Tyr}_{GUA}$ depletion represses cellular growth

Oxidative stress, a cellular stress with many known pleiotropic effects, results in cell growth repression through multiple pathways (Martindale and Holbrook, 2002). Consistent with previous work, we observed a robust growth defect in cells exposed to H_2O_2 (Fig 3.3A). We thus sought to determine if $tRNA^{Tyr}_{GUA}$ depletion might contribute to growth repression as a response to oxidative stress. We observed that impairment of $tRNA^{Tyr}_{GUA}$ function by either $tRNA^{Tyr}_{GUA}$ depletion or YARS depletion using two independent hairpins strongly impaired growth of MCF10A cells (Fig 3.3B). These results reveal that depletion of $tRNA^{Tyr}_{GUA}$ or inhibition of its cognate charging enzyme

can significantly impair growth and phenocopy the H_2O_2-induced physiological depletion of endogenous $tRNA^{Tyr}_{GUA}$.

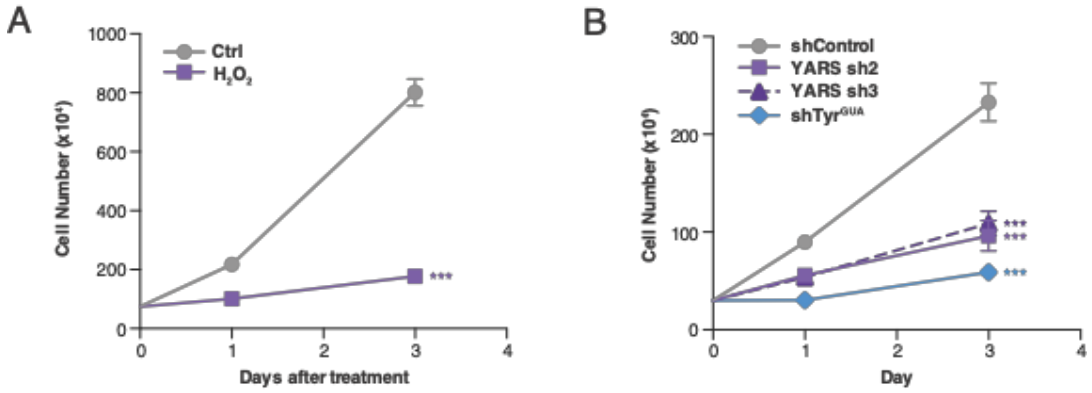

Figure 3.3. Depletion of $tRNA^{Tyr}_{GUA}$ contributes to the cell growth repression from oxidative stress

(A) Growth curves of MCF10A cells exposed to oxidative stress (200μM H_2O_2) relative to control cells (n=3). Two-way ANOVA was used to test for significance. (B) Growth curves of MCF10A cells expressing RNAi against mature $tRNA^{Tyr}_{GUA}$ or YARS relative to cells expressing a control hairpin (n=3). Two-way ANOVA was used to test for significance.

Data represent mean ± s.e.m.

As impaired $tRNA^{Tyr}_{GUA}$ was shown to repress cell growth, we wondered if overexpression of the tRNA could promote growth. After selection, northern blot showed no increase in mature $tRNA^{Tyr}_{GUA}$ in cells with a stably integrated vector for $tRNA^{Tyr}_{GUA}$ overexpression. A transient transfection with three concatenated tRNAs with upstream and downstream sequences included was shown to lead to tRNA overexpression

(Mattijssen et al., 2017). Interestingly, overexpression of $tRNA^{Tyr}_{GUA}$ was observed with the concatenated method only in case where the tRNA without an intron was included. With the intron present, overexpression of the pre-tRNA was observed but levels of the mature tRNA remained at control levels (Fig 3.4A-B). Following transfection of the tRNA without the intron, a significant increase in growth was observed in MCF10A cells (Fig 3.4C).

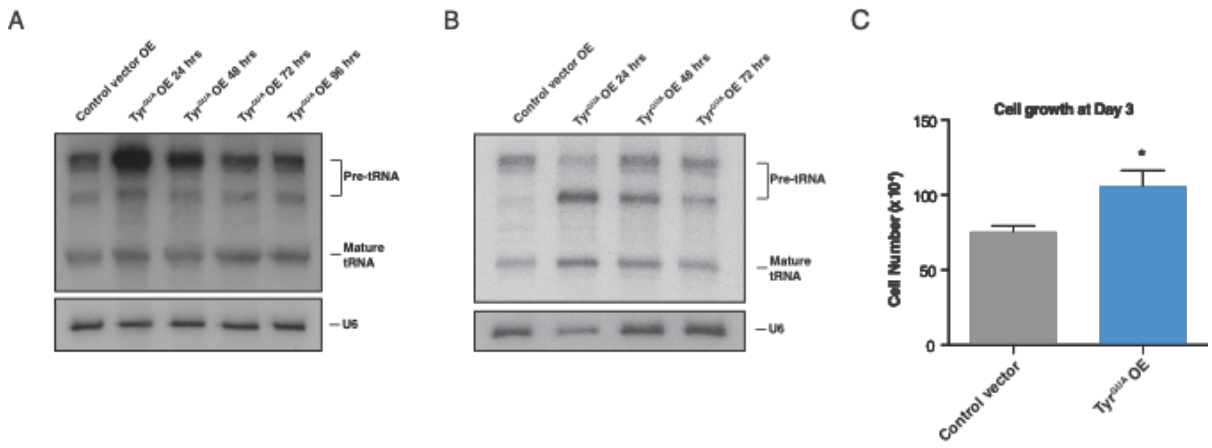

Figure 3.4. Overexpression of $tRNA^{Tyr}_{GUA}$ can promote cell growth

(A) Northern blot of MCF10A cells transiently transfected with a $tRNA^{Tyr}_{GUA}$ with intron overexpression vector relative to an empty control vector. The $tRNA^{Tyr}_{GUA}$ overexpression is shown at 24, 48, 72, and 96, hours post transfection. (B) Northern blot of MCF10A cells transiently transfected with a $tRNA^{Tyr}_{GUA}$ without intron overexpression vector relative to an empty control vector. The $tRNA^{Tyr}_{GUA}$ overexpression is shown at 24, 48, and 72 hours post transfection. (C) Cell growth of MCF10A cells transiently transfected with a $tRNA^{Tyr}_{GUA}$ overexpression vector relative to an empty control vector (n=3). A one-tailed Mann-Whitney test was used to test for significance at day 3.

Data represent mean ± s.e.m.

3.3 $tRNA^{Tyr}_{GUA}$ depletion represses expression of a set of growth genes

We hypothesized that stress-induced $tRNA^{Tyr}_{GUA}$ depletion impairs growth by reducing production of proteins enriched in its corresponding tyrosine codons. To search for such proteins, we conducted quantitative proteomic profiling of cells depleted of $tRNA^{Tyr}_{GUA}$ or impaired in $tRNA^{Tyr}_{GUA}$ aminoacylation. Label free mass-spectrometric proteomic profiling of cells depleted of $tRNA^{Tyr}_{GUA}$ or of YARS via shRNA-mediated knockdown revealed a highly significant correlation ($R=0.648$; $p < 2.2e\text{-}16$) in the proteomic profiles of these depleted cells relative to control hairpin expressing cells—consistent with a common set of downstream genes being impacted by these orthogonal methods of causing $tRNA^{Tyr}_{GUA}$ loss-of-function (Fig 3.5).

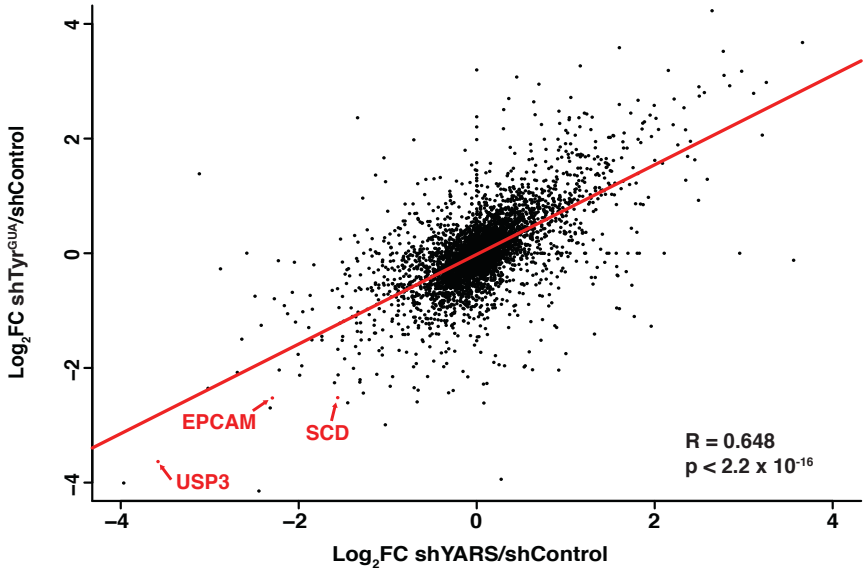

Figure 3.5. Proteomic profiling following tRNA$^{Tyr}_{GUA}$ depletion

A plot showing the correlation between protein abundance changes in the proteome upon either tRNA$^{Tyr}_{GUA}$ depletion or YARS depletion (shYARS-2) relative to control cells. A Pearson's two-sided test was used to test determine the statistical significance of the correlation between tRNA$^{Tyr}_{GUA}$ and YARS depletion effects across the detected proteome.

Amongst proteins that became depleted upon both of these perturbations, we searched for those that were also enriched for Tyr codons and are therefore likely to be tRNA$^{Tyr}_{GUA}$-dependent (Fig 3.6A). Using this approach, we identified 102 tyrosine-enriched proteins that exhibited sensitivity to tRNA$^{Tyr}_{GUA}$ depletion. This set of proteins was most significantly enriched in gene ontology (GO) functional categories (Ashburner

et al., 2000; The Gene Ontology, 2017) associated with cellular growth, including regulation of ATP synthesis, G0 to G1 cell-cycle progression, and phosphorylation (Table 3.1). These findings reveal that $tRNA^{Tyr}_{GUA}$ depletion represses the abundance of a set of proteins associated with growth.

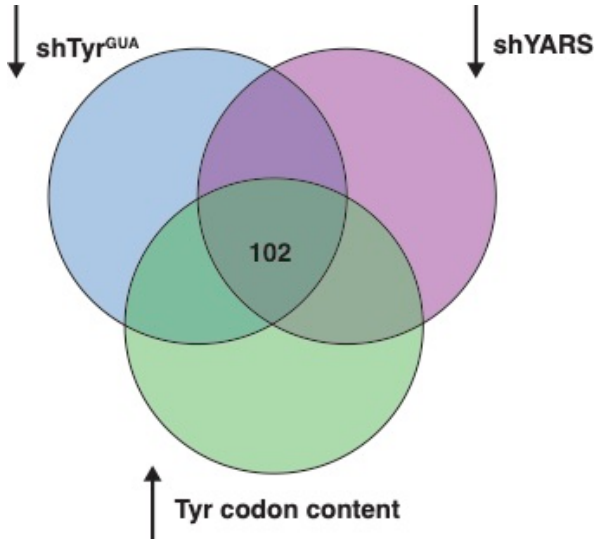

Figure 3.6. Identifying proteins that are most dependent on $tRNA^{Tyr}_{GUA}$ expression

Cells depleted of $tRNA^{Tyr}_{GUA}$ or YARS were processed for label free quantitation by mass spectrometry to identify proteins that were reduced by a $\log_2$-fold change of 0.5 or more. This set was overlapped with proteins containing a higher than median abundance of Tyr codon content to identify candidate mediators of the pleiotropic effects of $tRNA^{Tyr}_{GUA}$ depletion.

Table 3.1. GO functional analysis of Tyr-dependent proteins

GO terms	Description	p-value
GO:0042775	mitochondrial ATP synthesis coupled electron transport	3.30E-03
GO:0042773	ATP synthesis coupled electron transport	3.56E-03
GO:0007626	locomotory behavior	6.17E-03
GO:0070316	regulation of G0 to G1 transition	6.63E-03
GO:0045184	establishment of protein localization	6.65E-03
GO:0022904	respiratory electron transport chain	7.00E-03
GO:0006497	protein lipidation	8.98E-03
GO:0042475	odontogenesis of dentin-containing tooth	8.98E-03
GO:0042886	amide transport	9.17E-03
GO:0016310	phosphorylation	9.18E-03
GO:0006119	oxidative phosphorylation	9.42E-03

We selected a small set of $tRNA^{Tyr}_{GUA}$–regulated genes that exhibited some of the greatest fold reductions upon $tRNA^{Tyr}_{GUA}$ depletion for further functional studies (Fig 3.5). These genes comprised ubiquitin specific protease 3 (USP3), a hydrolase that deubiquitinates histone H2A and H2B and is required for mitotic entry and S phase progression (Nicassio et al., 2007), epithelial cell adhesion molecule (EPCAM), a tumorigenic cell surface protein over-expressed in many carcinomas (Munz et al., 2009), and stearoyl-CoA desaturase (SCD), the rate limiting enzyme for generating mono-unsaturated fatty acids such as palmitoleate and oleate—principle components of membrane phospholipids and cholesterol esters (Paton and Ntambi, 2009).

Quantitative western blotting revealed significant reductions in the endogenous levels of these proteins in cells upon shRNA-mediated depletion of $tRNA^{Tyr}_{GUA}$ or YARS (Fig 3.7A-B). In contrast, the control protein HSC70 was not significantly depleted, consistent with our proteomic findings of a specific set of proteins being modulated upon $tRNA^{Tyr}_{GUA}$ depletion. We also found mRNA levels by quantitative RT-PCR (qRT-PCR) of these 3 downstream genes to be reduced relative to the control cell line (Fig 3.7C). This result is most likely due to the destabilizing effects, as shown by others previously (Presnyak et al., 2015), that $tRNA^{Tyr}_{GUA}$ depletion has on mRNA as a tRNA that has become lower in abundance and non-optimal.

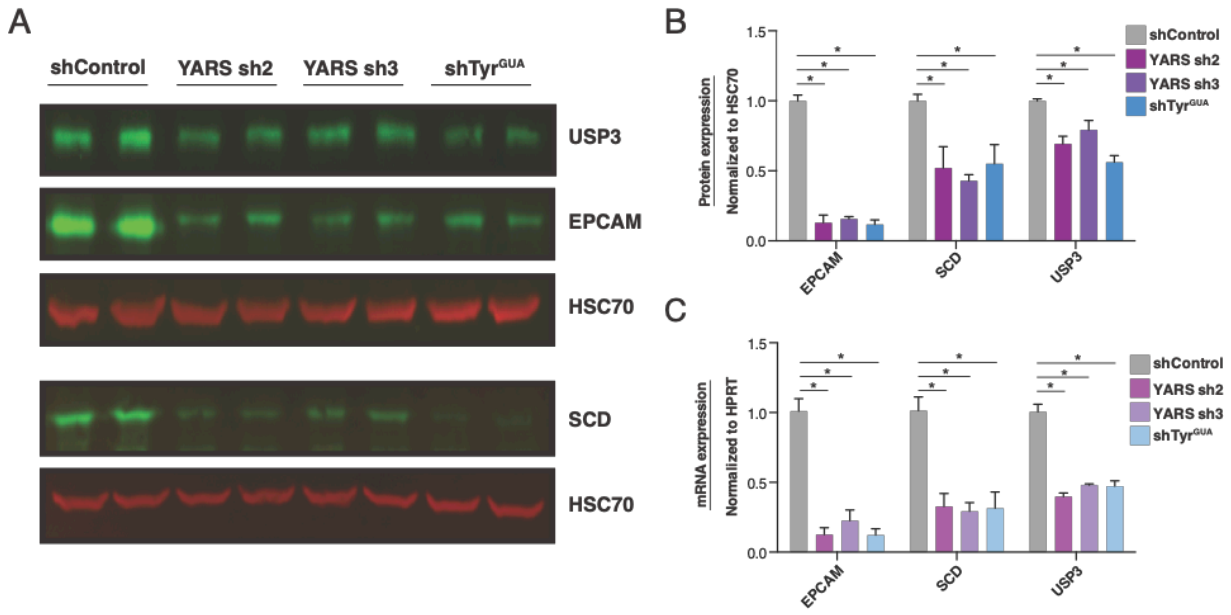

Figure 3.7. Validation of protein expression dependence on $tRNA^{Tyr}_{GUA}$ levels

(A) Quantitative western blot validation depicting abundances of protein targets (EPCAM, SCD, and USP3) identified from proteomic profiling. HSC70 was used as a loading control and is not modulated upon molecular perturbation of $tRNA^{Tyr}_{GUA}$. (B) Quantification of western blot analysis in (A) (n=4). A one-tailed Mann-Whitney test was used to test for statistical significance between knockdown and control conditions. (C) Levels of mRNA expression for target genes in cells depleted of either $tRNA^{Tyr}_{GUA}$ or YARS as measured by qRT-PCR (n=4). A one-tailed Mann-Whitney test was used to test for statistical significance between the knockdown and control cell lines' gene expression values.

Data represent mean ± s.e.m.

To determine if repressed expression of these genes indeed impairs proliferation, we depleted these genes via RNAi. Knockdown of each of these genes by two independent hairpins (Fig 3.8) repressed the growth of MCF10A cells—consistent with growth-promoting roles for these genes (Fig 3.9).

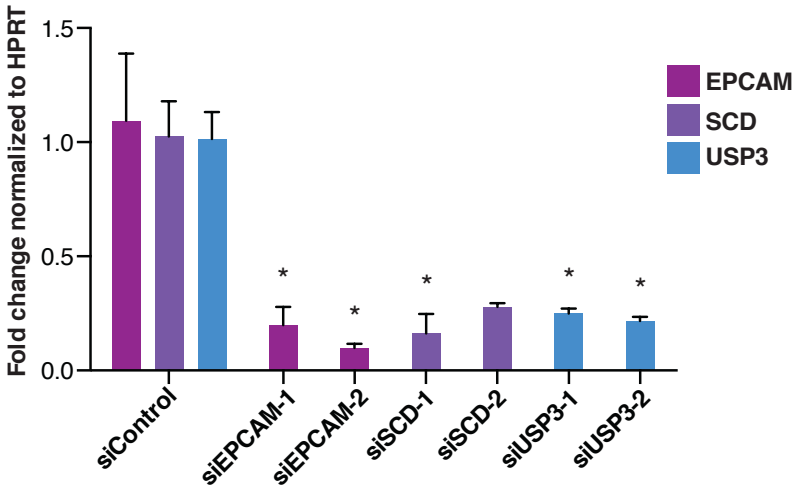

Figure 3.8. Expression of EPCAM, SCD, and USP3 with siRNA-mediated knockdown

Total mRNA from MCF10A cells transiently transfected with two independent siRNA targeting EPCAM, SCD, or USP3 was analyzed by quantitative RT-PCR at the end of each growth assay. A one-tailed Mann-Whitney test was used to establish statistical significance (n=3 except for siSCD-2 has n=2).
Data represent mean ± s.e.m. *$p < 0.05$

Our results reveal that repressing the function of a specific tRNA by depleting it or inhibiting its aminoacylation, and thus its use in translation, represses expression of a

set of tyrosine enriched proteins enriched in growth-dependent processes. Moreover, depletion of $tRNA^{Tyr}_{GUA}$ or its downstream regulated genes impairs growth of breast epithelial cells. We propose that this network constitutes a pro-growth $tRNA^{Tyr}_{GUA}$-regulated pathway and its repression via oxidative stress-induced tRNA fragmentation and depletion constitutes an adaptive growth suppressive stress response.

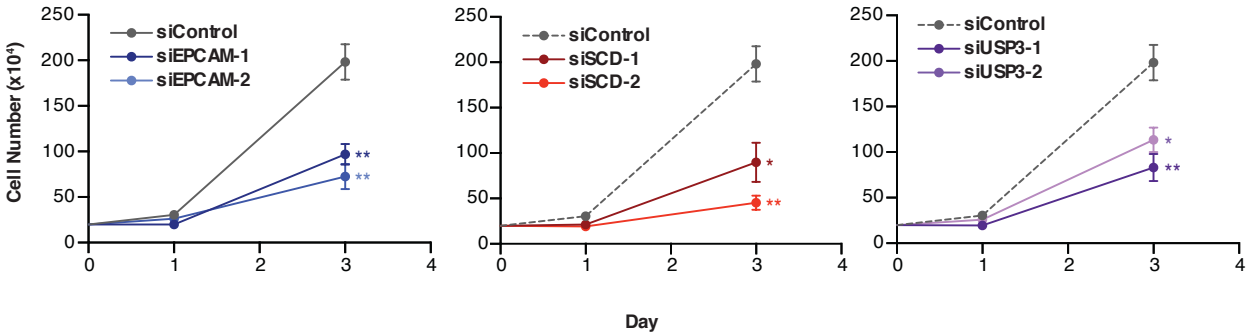

Figure 3.9. EPCAM, SCD, and USP3 promote cell growth

Growth curves for MCF10A cells were transfected with either control siRNA or two independent siRNA targeting EPCAM, SCD, or USP3. Note that the control cell growth curve is the same in all graphs and were plotted separately for clarity and does not represent independent experiments. Two-way ANOVA was used to test for significance. Data represent mean ± s.e.m. *$p < 0.05$ and **$p < 0.01$

3.4 $tRNA^{Tyr}_{GUA}$ depletion impairs protein translation in a codon-dependent manner

Our findings indicate that the abundance of cellular $tRNA^{Tyr}_{GUA}$ levels regulates the protein levels of a set of growth-associated genes enriched in tyrosine codons. We

hypothesized that these proteins would also be sensitive to oxidative stress-induced $tRNA^{Tyr}_{GUA}$ depletion. To test if our target proteins become repressed upon oxidative stress, we used quantitative western blotting 24 hours after H_2O_2 treatment, a time point when $tRNA^{Tyr}_{GUA}$ is depleted. Consistent with our previous experiments, we noted significant reductions in the protein levels of these $tRNA^{Tyr}_{GUA}$-regulated genes (Fig 3.9A-B). Despite these reductions at the protein level, qRT-PCR of these H_2O_2 treated cells showed no significant change for two out of the three downstream targets (Fig 3.9C) relative to the control, suggesting that $tRNA^{Tyr}_{GUA}$ depletion can regulate protein expression at the level of translation. Similar to other situations in biology, it appears as though the effect on the downstream proteins occurs through multiple layers of regulation and that $tRNA^{Tyr}_{GUA}$ depletion can act through mRNA destabilization as well as through translational repression.

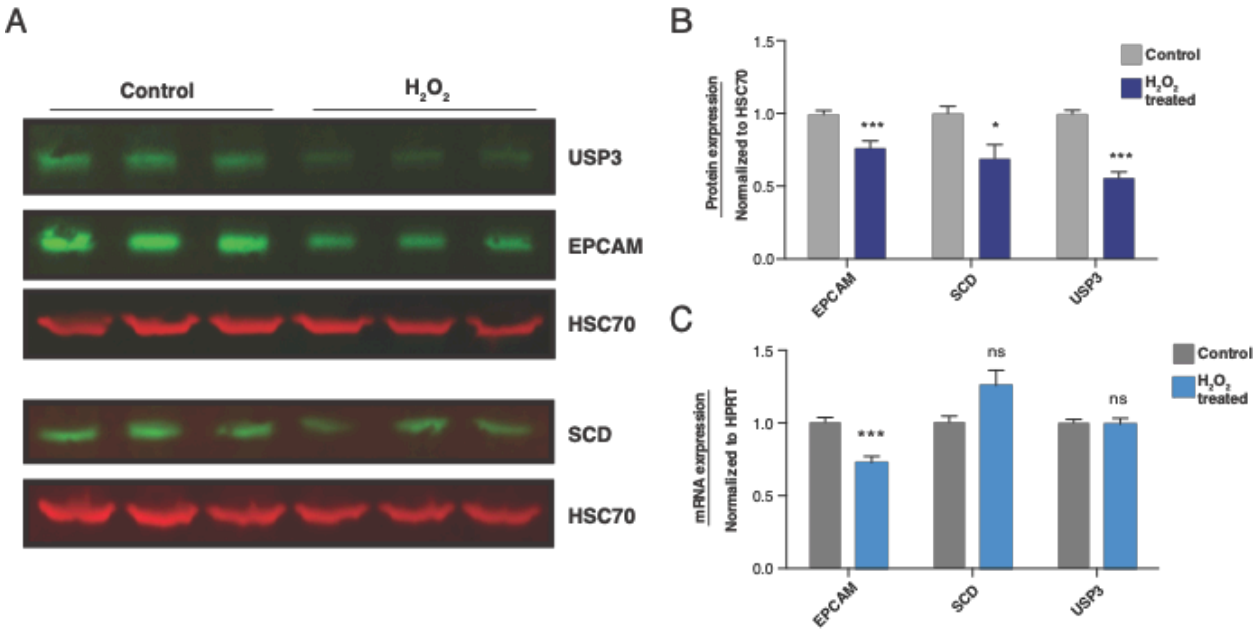

Figure 3.10. Protein levels of EPCAM, SCD, and USP3 following oxidative stress

(A) Quantitative western blot EPCAM, SCD, and USP3 in MCF10A cells 24 hours after treatment with H_2O_2 (200μM). HSC70 was used as a loading control. (B) Quantification of western results in (A) (n=9). A one-tailed Mann-Whitney test was used to establish statistical significance between treated and control conditions. (C) Levels of mRNA expression for target genes 24 hours after treatment with H_2O_2 (200μM) as measured by qRT-PCR (n=9). A one-tailed Mann-Whitney test was used to test for statistical significance between the treated and control cell lines' gene expression values. Data represent mean ± s.e.m.

To further test if $tRNA^{Tyr}_{GUA}$ depletion can act at the level of translation, took two different experimental approaches. The first method was a codon-dependent reporter of an endogenous target of $tRNA^{Tyr}_{GUA}$ depletion. A Myc-tagged USP3 was cloned upstream of Luciferase, which acted as a transfection control. This USP3 was either a wild-type (WT) or a mutant construct that had 5 tyrosine codons mutated to alanine codons (Fig 3.10A). We hypothesized that by reducing the number of tyrosine codons present in the gene, the mutant would be less susceptible to reduced protein expression following $tRNA^{Tyr}_{GUA}$ depletion. These reporters were transfected into MCF10A cells and 24 hours after H_2O_2 treatment and quantitative western blotting was performed. Consistent with our model of a codon-dependent regulation at the level of translation, we noted a significant increase in the abundance of the mutant USP3 compared to the WT protein (Fig 3.10B).

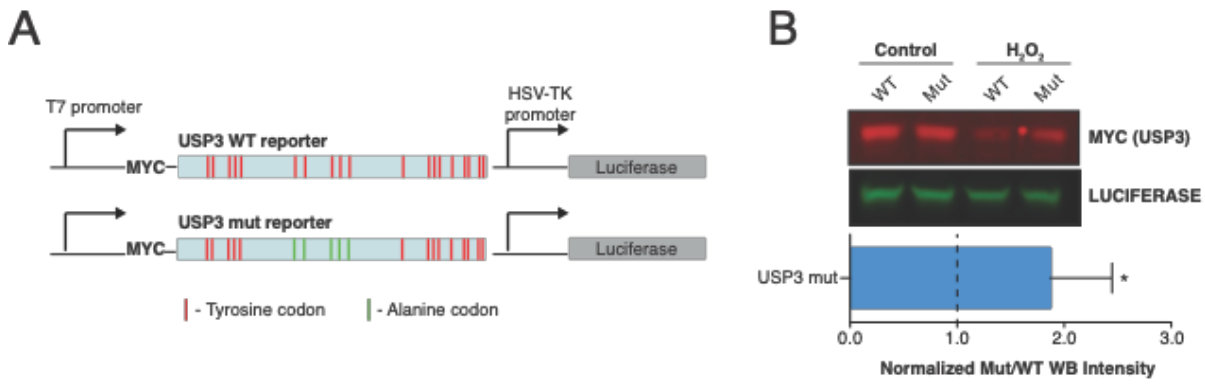

Figure 3.11. A codon-based reporter following $tRNA^{Tyr}_{GUA}$ depletion

(A) A schematic of the codon-based USP3 reporter. A Myc-tagged WT or mutant reporter with 5 Tyr codons mutated to Ala codons were cloned upstream of a Luciferase used for transfection normalization. (B) Quantitative western blot for the Myc-tag and Luciferase (top) with the normalized fluorescent intensities (bottom) are shown (n=3). Data represent mean ± s.e.m. *$p < 0.05$

Though our reporter showed a clear likelihood of codon-dependent regulation of translation for USP3, we wondered if this occurred on a global scale in the cell following $tRNA^{Tyr}_{GUA}$ depletion. Protein expression levels of EPCAM, SCD, and USP3 were sensitive to both the abundance of $tRNA^{Tyr}_{GUA}$ as well as its charging enzyme—implicating modulation of ribosomal translation of this gene set in a $tRNA^{Tyr}_{GUA}$ and tyrosine codon-dependent manner. To directly test if ribosomal engagement of tyrosine-codon enriched transcripts is impaired upon $tRNA^{Tyr}_{GUA}$ depletion, our second

experimental approach was to perform ribosomal profiling in control and $tRNA^{Tyr}_{GUA}$–depleted cells (Ingolia et al., 2009).

We compared the ribosome protected fragments (RPFs) detected in cells with and without $tRNA^{Tyr}_{GUA}$ depletion, in order to examine the global translational effects due to modulating a single tRNA. We observed similar length distribution and nucleotide periodicity for ribosome-protected fragments as those of previous studies (Fig 3.11A-B) (Ingolia et al., 2009; Lareau et al., 2014; McGlincy and Ingolia, 2017).

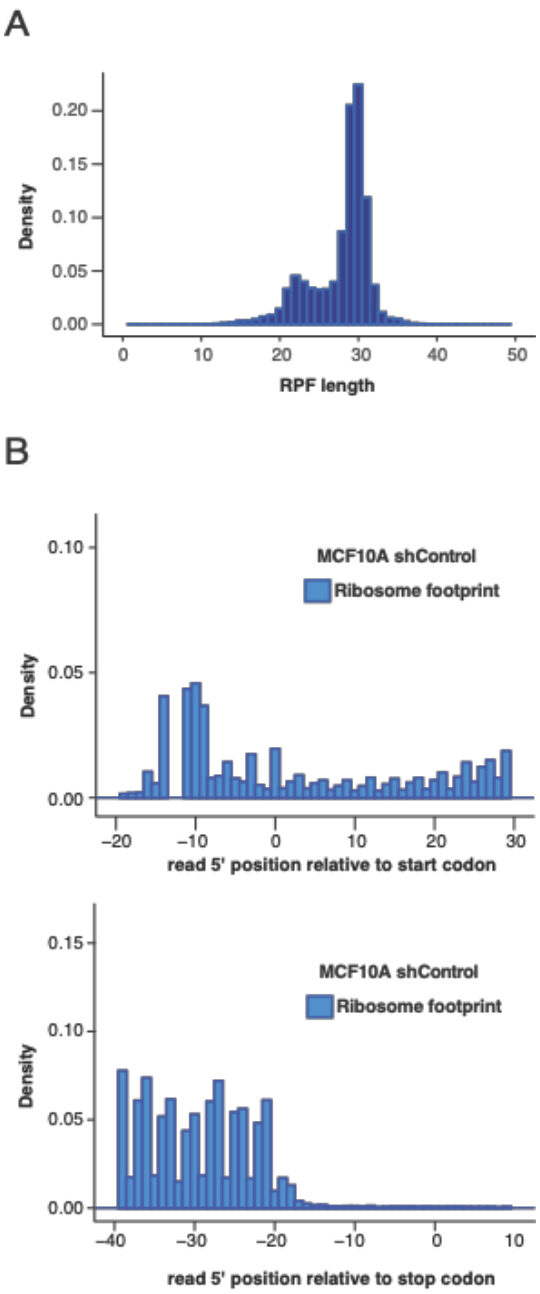

Figure 3.12. Ribosome protected fragments are the expected size and show a 3-nucleotide periodicity

(A) Histogram of the read length distribution of ribosome protected fragments observed upon ribosome profiling sequence analysis. (B) Examples of the mapped position of the 5'-end of reads near the start (top) or stop (bottom) codons are shown, revealing the characteristic 3-nucleotide periodicity of ribosomal positioning observed as previously described by (Ingolia et al., 2009).

A corrected ribosome-occupancy score was calculated for each gene as a metric for active translation in control and $tRNA^{Tyr}_{GUA}$–depleted cells. We observed that $tRNA^{Tyr}_{GUA}$–depletion caused a significant reduction in ribosome engagement of transcripts significantly enriched in UAC and UAU—the codons cognate to $tRNA^{Tyr}_{GUA}$. Genes with distinct translation efficiencies, defined as the ratio between RPFs and mRNA fragments, were separated into three equally populated gene sets. Genes with higher tyrosine codons were significantly enriched in the set of genes with the lowest translational efficiency (denoted by the lowest red bar in Fig 3.12) upon $tRNA^{Tyr}_{GUA}$ depletion (Fig 3.12). These findings reveal that ribosomal translation of a set of tyrosine codon-enriched genes in these mammalian cells is sensitive to $tRNA^{Tyr}_{GUA}$ levels.

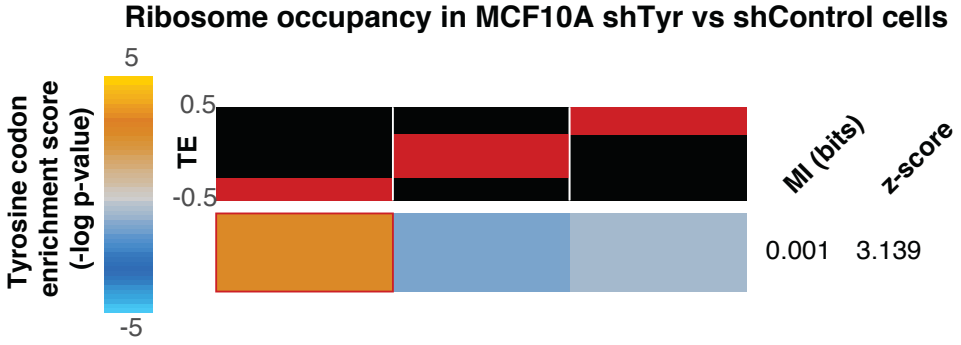

Figure 3.13. Decreased translational efficiency is observed in tyrosine-rich genes following $tRNA^{Tyr}_{GUA}$ depletion

Genes were sorted based on their changes in GC-corrected translation efficiency (TE) values, with reduced TE in $tRNA^{Tyr}_{GUA}$-depleted cells shown in left and enhanced TE shown on right. The red bars over each column depict the range of values in that bin. We then assessed the distribution of genes with high tyrosine codon content across these three bins using mutual information calculation and testing (see methods for details). For visualization, we used the hypergeometric distribution to assign p-values to the overlap between tyrosine-rich genes and each of the three bins. We then defined an enrichment score as –log of p-value, if there was a significant enrichment. If the overlap is significantly fewer than expected by chance, log of p-value is used instead (depletion). The resulting enrichment score is then shown as a heatmap with gold depicting positive enrichment.

3.5 Summary

In this chapter, the effects of $tRNA^{Tyr}_{GUA}$ depletion following oxidative stress are further explored. The depletion of $tRNA^{Tyr}_{GUA}$ leads to decreased protein expression of a subset of $tRNA^{Tyr}_{GUA}$-sensitive targets at both the transcriptional and translational level. These effects were experimentally confirmed through a combination of mass spectrometry, ribosome profiling, and a codon-based reporter that all showed the widespread consequences of the depletion of a single tRNA. Some of the most affected proteins, EPCAM, SCD, and USP3, were validated and reduction of these proteins and $tRNA^{Tyr}_{GUA}$ were shown to contribute to the repression of cell growth seen in response to oxidative stress.

CHAPTER 4: Characterization and Functional Analysis of the Stress-Induced tRF^{Tyr}

In response to oxidative stress, we observed a rapid induction of the tRF$^{Tyr}_{GUA}$ followed by a delayed reduction in levels of tRNA$^{Tyr}_{GUA}$. Previously, tRFs have been found to be functional and regulate gene expression, ribosome biogenesis, translation initiation, as well as other functions (Chen et al., 2016; Goodarzi et al., 2015; Kim et al., 2017; Sharma et al., 2016; Yamasaki et al., 2009). Given that numerous other tRFs have been found to be functional, we wondered if the tRF$^{Tyr}_{GUA}$ induced by oxidative stress was also functional. In this chapter, we use multiple experiments to both characterize the tRF as well as verify interactions with RNA binding proteins. We then show a functional role for this tRF and our data helps shed light on why this response is seen so quickly following oxidative stress.

Understanding the role of tRFs represents an exciting new field of RNA biology as it holds the potential for many discoveries. Initial findings show that tRFs can be highly abundant, as their precursor molecules are also highly abundant, and can be immediately induced. Our results, consistent with other findings (Kirchner and Ignatova, 2015), show that the response of tRFs can happen on the scale of minutes, substantially quicker than transcriptional level changes. By northern blot, we can see the induction of the tRF$^{Tyr}_{GUA}$ within minutes of oxidative stress. Moreover, our initial smRNA-seq data shows that numerous other tRFs are induced, each with the capability of being functional. Though the data in this chapter continue to add to the growing body

of understanding tRFs, it's reasonable to think that we have only begin to scratch the surface of the possibilities that tRFs might play in RNA and cellular biology.

4.1 Characterization of the stress-induced tRF$^{Tyr}_{GUA}$

In addition to causing tRNA$^{Tyr}_{GUA}$ depletion, oxidative stress also induced generation of tRF$^{Tyr}_{GUA}$ (Fig 2.5). Though this induction was seen within minutes of oxidative stress, the tRF remained present for hours at elevated levels in the cell (Fig 4.1A-B).

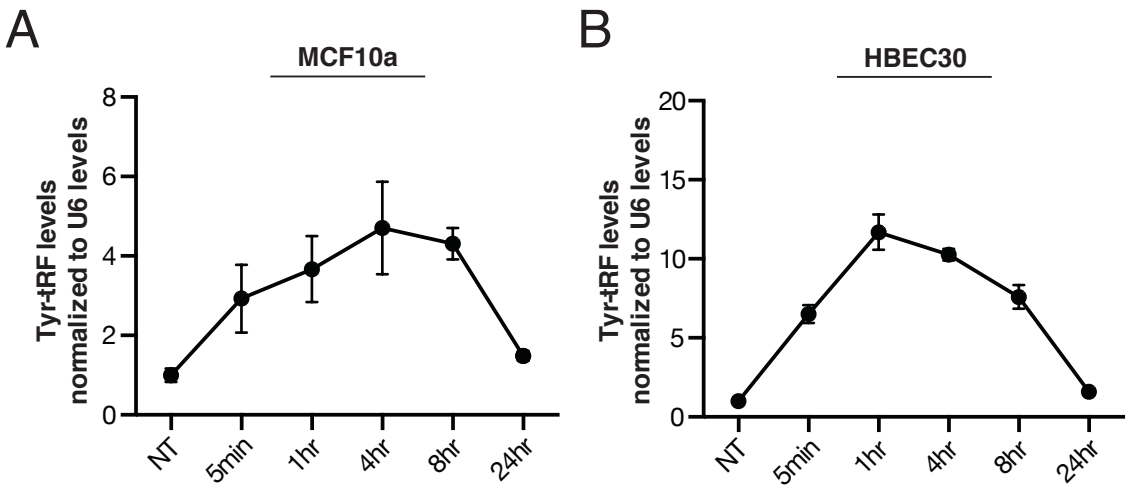

Figure 4.1. Elevated levels of tRF$^{Tyr}_{GUA}$ after oxidative stress

(A-B) Quantification of tRF$^{Tyr}_{GUA}$ induction in response to oxidative stress as a function of time in MCF10A (A) (n=4) and in HBEC30 (B) (n=6). A similar response and time course is seen in the two cell lines. Following oxidative stress, tRF$^{Tyr}_{GUA}$ remained elevated for hours before returning to baseline levels at 24 hours post exposure.

Furthermore, we wondered whether this tRF originated from a single precursor or multiple as many genomic loci are present for $tRNA^{Tyr}_{GUA}$. Sequencing of the tRF^{Tyr}_{GUA} after gel extraction identified tRFs with a 5' leader sequence from nearly every $tRNA^{Tyr}_{GUA}$ genomic locus (Fig 4.2A-B), confirming that the pre-tRNA is the original source of tRF^{Tyr}_{GUA}. While all tRFs had the 5' exon sequence in common, the majority of tRFs appeared to stop at the intron start site. Interestingly, some of the tRF^{Tyr}_{GUA} appeared to include parts of the intron. Our sequencing lacks the quantitative power to conclusively identify the abundance of a tRF from a given locus relative to others, but it seems likely that tRFs from multiple loci are present at appreciable quantities following oxidative stress.

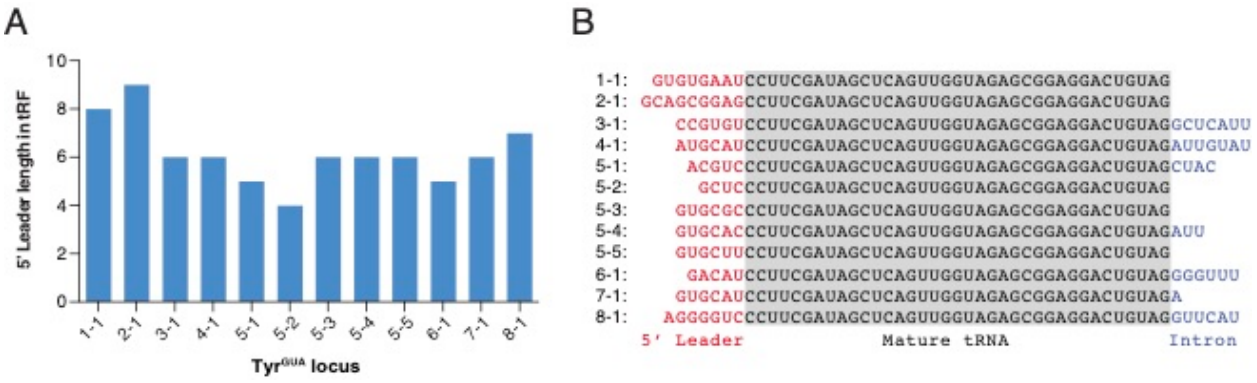

Figure 4.2. Sequencing of the tRF confirms it derives from the pre-$tRNA^{Tyr}_{GUA}$

(A) Length of 5' leader sequence of all tRF^{Tyr}_{GUA} by loci that were identified by sequencing. Although the length of the remaining leader sequence varied by tRF, all tRFs contained one. (B) Sequence of each tRF^{Tyr}_{GUA} by loci that were identified by sequencing. Conserved tRF^{Tyr}_{GUA} sequences from the 5' mature exon found in each loci are highlighted in gray. Leader and intronic sequences found in the tRF have no sequence conservation.

4.2 Angiogenin and defective tRNA splicing are not the sources of tRF^{Tyr}_{GUA}

Sequencing of the tRF^{Tyr}_{GUA} after gel extraction identified tRFs with a 5' leader sequence from nearly every $tRNA^{Tyr}_{GUA}$ genomic locus (Fig 4.2). As the tRF originates from the pre-tRNA, we speculated that the tRNA splicing machinery might be involved in the induction of this fragment. In order to test this, we used siRNA-mediated knockdown for TSEN2, the catalytic subunit of the tRNA splicing complex (Paushkin et al., 2004), as well as for angiogenin (ANG), one of the best-characterized RNases to cleave tRNAs at the anticodon loop (Fu et al., 2009). Although ANG has been observed to cleave mature tRNAs, it remains unclear whether this enzyme is able to recognize and cleave pre-tRNAs.

We used siRNA-mediated knockdown of both TSEN2 and ANG as an acute reduction in the levels of these proteins would limit any compensatory effects. After transfection of siRNA, we exposed MCF10A cells to oxidative stress and examined, by northern blot, whether any tRF^{Tyr}_{GUA} was observed. Surprisingly, we observed an equal level of tRF induction with knockdown of either ANG or TSEN2, suggesting that these two ribonucleases were not mediating our effect (Fig 4.3A-C).

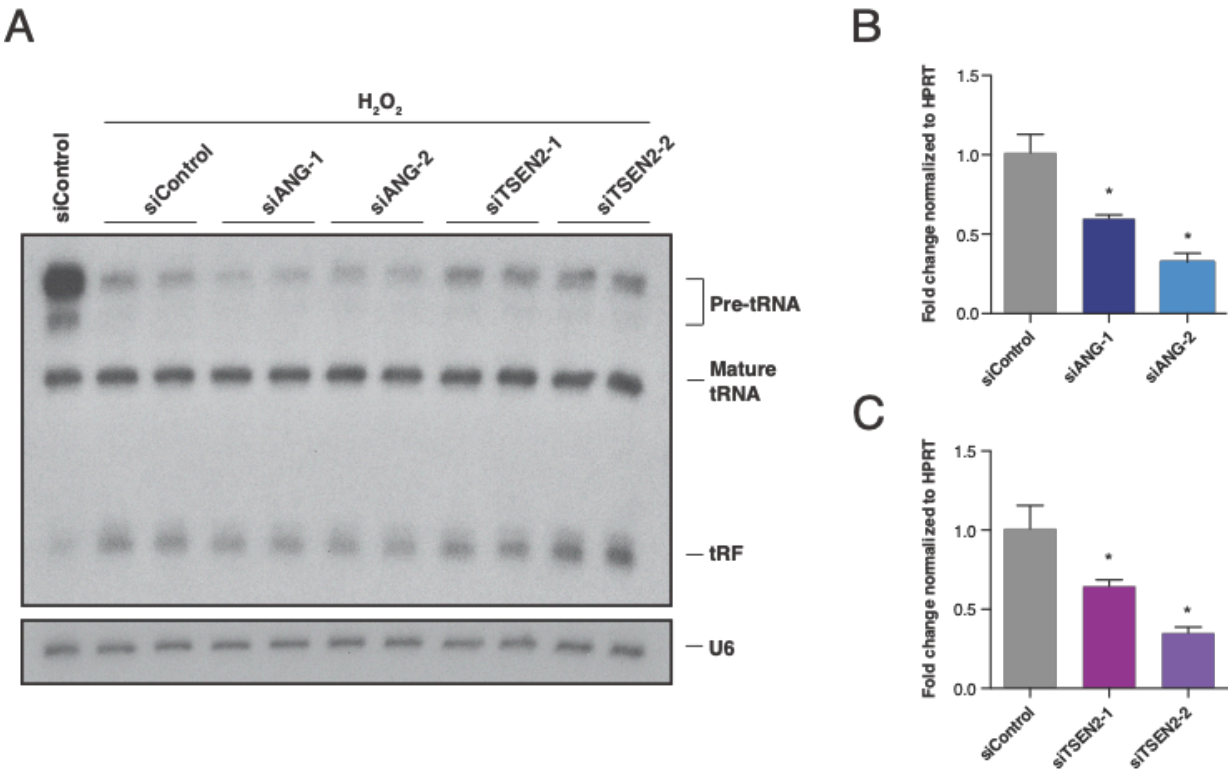

Figure 4.3. Angiogenin and TSEN2 are not involved in tRF^{Tyr}_{GUA} induction in response to oxidative stress

(A) A northern blot depicting the tRF^{Tyr}_{GUA} induction in MCF10A cells with two independent siRNA each against angiogenin (ANG) or TSEN2 relative to a control siRNA. (B) A qRT-PCR validation of the siRNA-mediated knockdown of ANG relative to a control siRNA (n=4). (C) A qRT-PCR validation of the siRNA-mediated knockdown of TSEN2 relative to a control siRNA (n=4).

Data represent mean ± s.e.m.

Further evidence suggesting that a defect in tRNA splicing was not the source of the tRF induction was that equal levels of tRFs were seen following RNAi-mediated knockdown of the RNA kinase CLP1 (Fig 4.4A-B). CLP1 is responsible for phosphorylating the ends of the mature tRNA exons to allow for ligation after intron removal and this kinase, similar to TSEN2, is a component of the tRNA splicing complex (Weitzer and Martinez, 2007). Our data argues against ANG and the tRNA splicing complex from being responsible for this tRF^{Tyr}_{GUA} induction after oxidative stress and future studies will be necessary to identify the RNase or RNases involved in this stress response pathway.

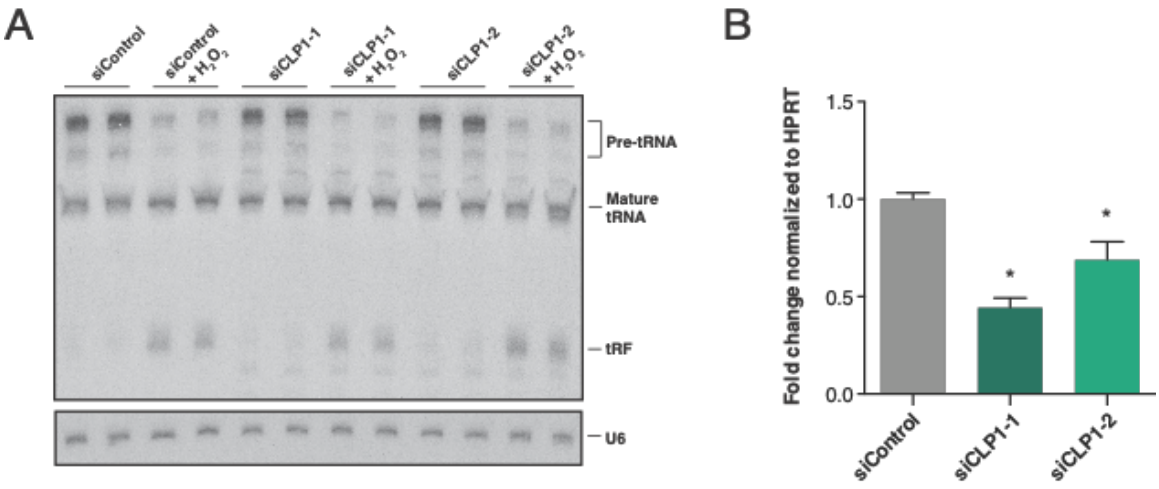

Figure 4.4. CLP1 and tRNA splicing are not involved in tRF^{Tyr}_{GUA} induction in response to oxidative stress

(A) A northern blot depicting the tRF^{Tyr}_{GUA} induction in MCF10A cells with two independent siRNA against CLP1 relative to a control siRNA. (B) A qRT-PCR validation of the siRNA-mediated knockdown of CLP1 relative to a control siRNA (n=4). Data represent mean ± s.e.m.

4.3 A synthetic mimetic of tRF$^{Tyr}_{GUA}$ is used to identify interacting factors

We next sought to identify if this tRF$^{Tyr}_{GUA}$ might function in the same pathway as the mature tRNA. Using the conserved, and most likely functional, sequence from the different sequenced tRF$^{Tyr}_{GUA}$ (Fig 4.2B), we transfected a 37nt synthetic mimetic as a method of overexpression. However, overexpression of tRF$^{Tyr}_{GUA}$ resulted in no significant change in cell growth (Fig 4.5A) or in the protein expression of USP3, SCD, or EPCAM (Fig 4.5B). If this tRF were to have regulatory functions, our data suggested it might play a role in an independent pathway. One mechanism by which tRFs have been proposed to function is through their interaction with various RNA binding proteins (RBPs) (Couvillion et al., 2010; Goodarzi et al., 2015; Haussecker et al., 2010).

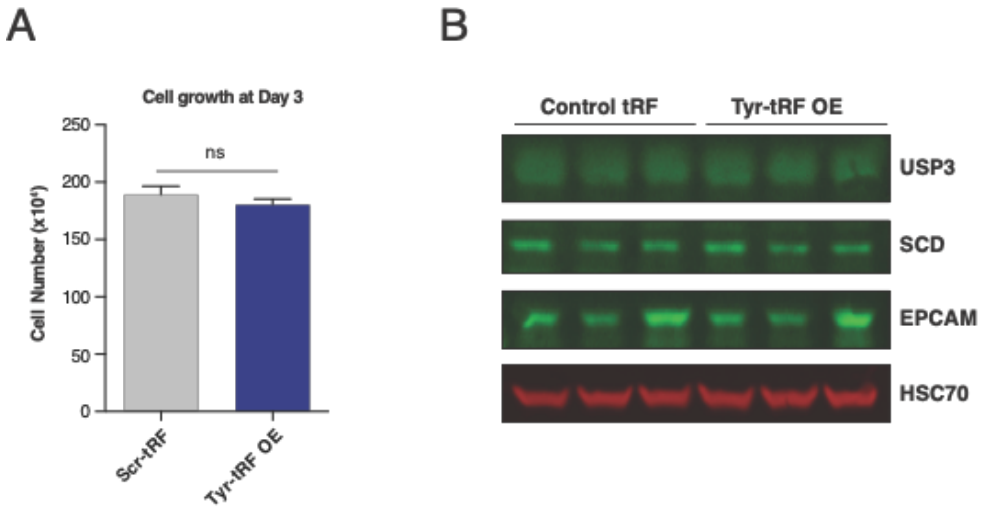

Figure 4.5. The tRF^{Tyr}_{GUA} is not involved in the same pathway as $tRNA^{Tyr}_{GUA}$ depletion.

(A) Cell growth of MCF10A cells transiently transfected with a tRF^{Tyr}_{GUA} mimetic relative to a scrambled tRF control (n=3). A one-tailed Mann-Whitney test was used to test for significance at day 3. (B) Western blot of downstream $tRNA^{Tyr}_{GUA}$-dependent genes 24 hours after transfection of tRF^{Tyr}_{GUA} mimetic or a scrambled tRF control.
Data represent mean ± s.e.m.

We hypothesized that tRF^{Tyr}_{GUA} may not only be a product of tRNA fragmentation, but may also interact in *trans* with an RBP. To test this, we used a synthetic tRF^{Tyr}_{GUA} as bait in an *in vitro* co-precipitation experiment where the 5'-biotinylated tRF mimetic was captured on streptavidin beads and then incubated with cellular lysate. Proteins interacting with the mimetic were identified by in-solution digestion and mass-spectrometry, and compared to proteins interacting with a

scrambled mimetic. Mass spectrometry identified numerous proteins that were enriched in the tRF^{Tyr}_{GUA} co-precipitation relative to scrambled control oligonucleotide (Fig 4.6). We selected the most significantly enriched proteins—hnRNPA0, hnRNPA1, and SSB—and validated their interaction with synthetic tRF^{Tyr}_{GUA} by western blot. Western blot analyses confirmed the mass spectrometry results, showing increased interactions between these proteins and tRF^{Tyr}_{GUA} mimetic relative to scrambled control (Fig 4.7). These results suggest that tRF^{Tyr}_{GUA} may interact with one or more RBPs.

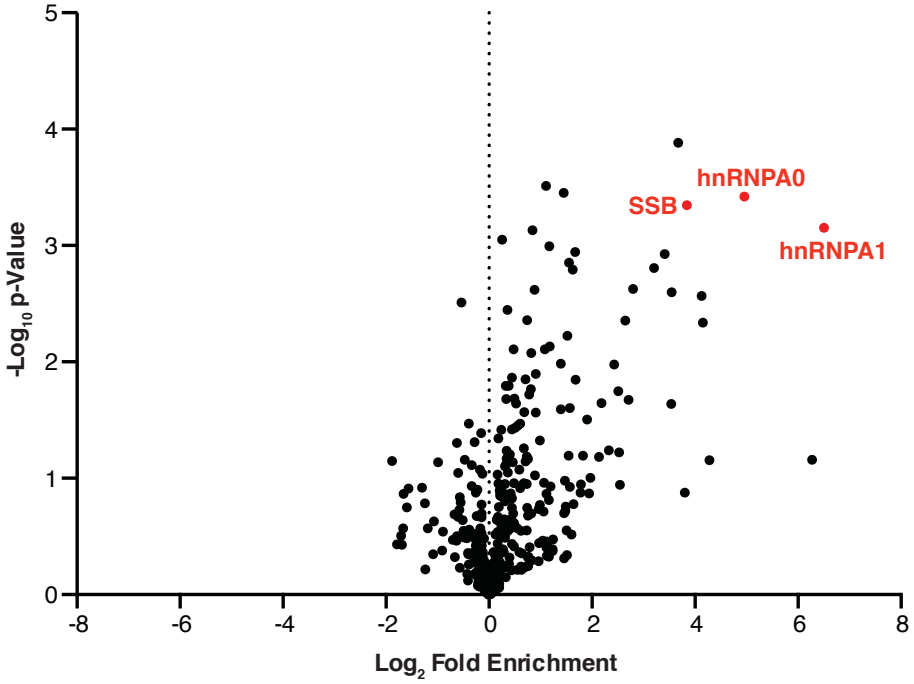

Figure 4.6. Identifying tRF-interacting RBPs using mass spectometry

Volcano plot of mass spectrometry results from a synthetic 5'-biotinylated tRF^{Tyr}_{GUA} co-precipitation experiment with cell lysate. Log_2 fold enrichment values of proteins identified from tRF^{Tyr}_{GUA} relative to scrambled tRF control samples. Three of the most enriched and most significant results (red) were chosen for further study.

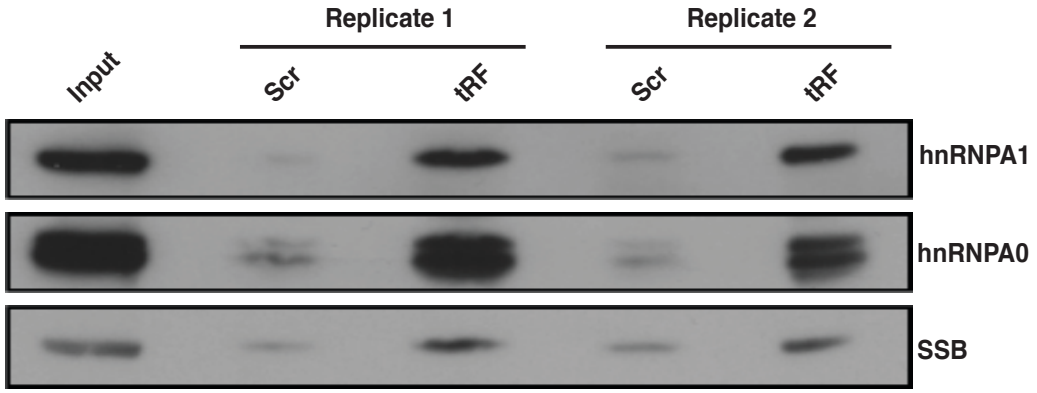

Figure 4.7. Western blot validation of the mass spectrometry results
Western blot validation of mass spectrometry results for three of the top hits in Fig 4.6, showing co-precipitation of endogenous proteins with transfected tRF^{Tyr}_{GUA} relative to a scrambled control sequence (Scr).

4.4 Validation of an endogenous in vivo interaction between tRF^{Tyr}_{GUA} and the RBPs, hnRNPA1 and SSB

We next sought to determine if there is an endogenous interaction between tRF^{Tyr}_{GUA} and an RBP. UV-crosslinking enables assessment of direct endogenous interactions between RBPs and their cellular RNA substrates (Mili and Steitz, 2004; Ule et al., 2003) and has been coupled with deep-sequencing methods such as HITS-CLIP or PAR-CLIP to identify the landscape of RNAs that interact with a given RBP (Hafner et al., 2010; Licatalosi et al., 2008). The initial steps of such CLIP-sequencing approaches

require limited RNase digestion of immunoprecipitated ribonucleoprotein complexes prior to SDS-PAGE visualization. Such experiments have previously been done with Argonaute-2, which binds microRNAs (Chi et al., 2009), and YBX1, which binds tRFs (Goodarzi et al., 2015). These experiments have revealed well-defined bands roughly the size of the RBP, which show the RBP bound to a population of small RNAs. In contrast, for RBPs that bind mRNAs, CLIP-seq methods reveal a smear that indicates the RBP bound to a population of longer RNAs (Chi et al., 2009; Goodarzi et al., 2015) (Fig 4.8).

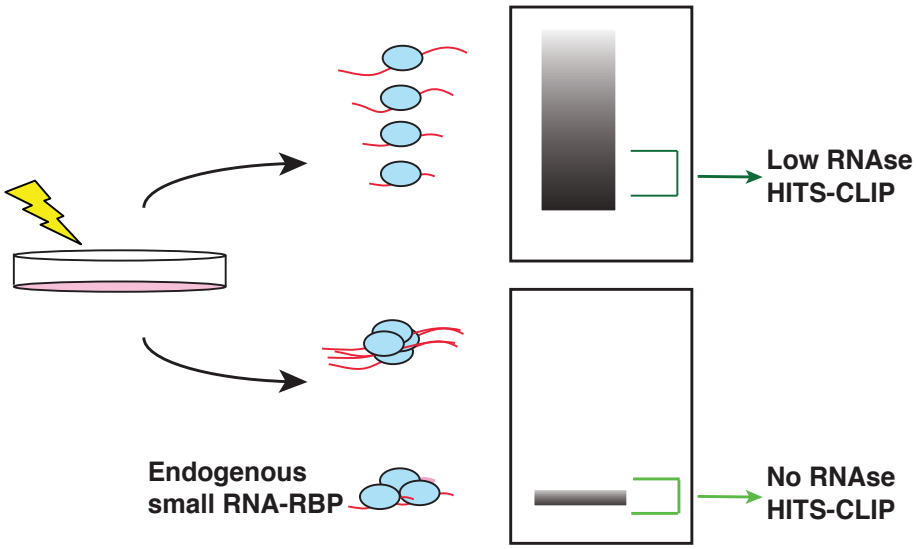

Figure 4.8. A schematic of HITS-CLIP for smRNAs

Schematic depicting the expected visualization of a cross-linked immunoprecipitation by autoradiogram. Samples processed in the absence of RNase digestion that revealed a band corresponding to smRNA-RBP interactions were processed for HITS-CLIP. Samples processed using low RNase digestion showing a smear representing mRNA-RBP interactions by autoradiogram were also processed for HITS-CLIP.

To determine if any of the candidate RBPs identified by mass spectrometry interact with endogenous small RNA populations, we included an experimental condition where the HITS-CLIP protocol was conducted in the absence of RNase digestion to ensure that any potential small RNA-RBP bands visualized were not a consequence of, or confounded by, RNase digestion. UV-crosslinked immunoprecipitation followed by SDS-PAGE in the presence or absence of RNase digestion revealed that endogenous hnRNPA1 and SSB interacted with an endogenous small RNA population (Fig 4.9A-B). We did not observe a small RNA-ribonucleoprotein band for hnRNPA0 in the absence of RNase (Fig 4.9C), even upon prolonged autoradiographic exposure, suggesting that this RBP either does not significantly interact with a small RNA population *in vivo* or this method is not conducive to identifying this interaction. These findings suggest that hnRNPA1 and SSB directly interact with small RNA populations *in vivo*.

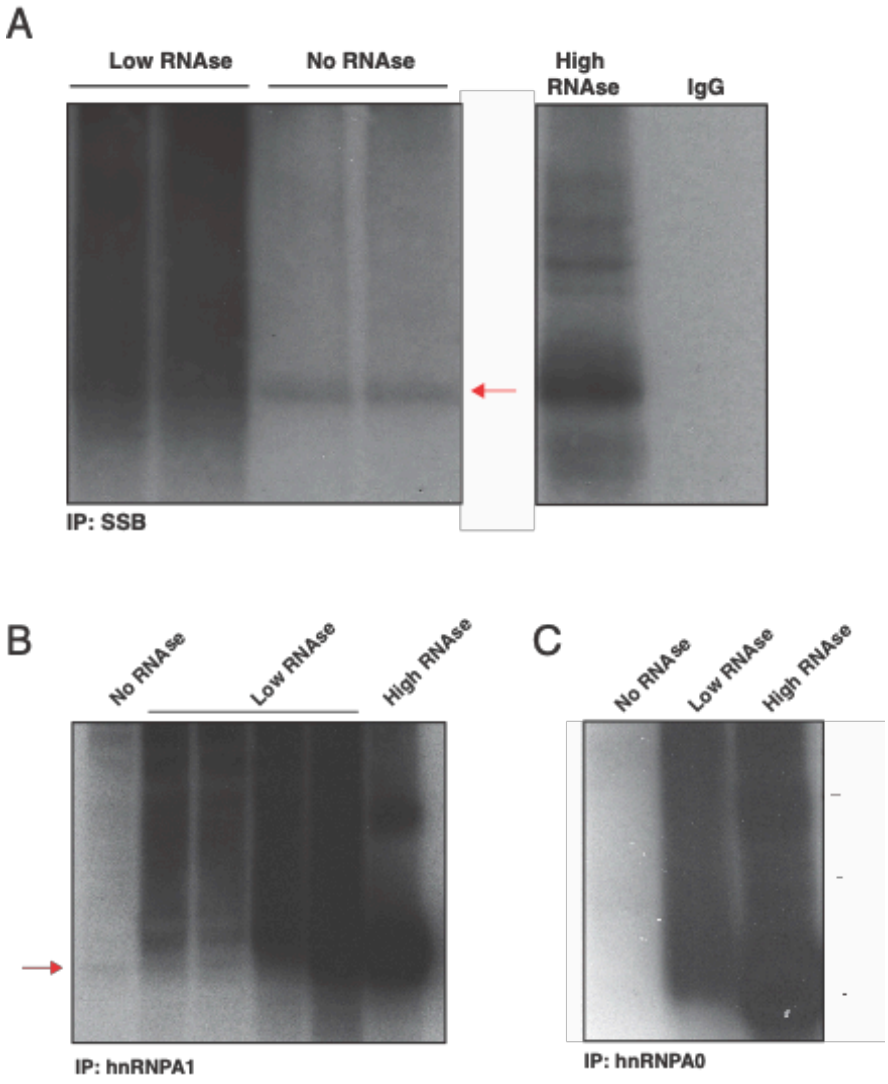

Figure 4.9. Autoradiograms to detect interactions with endogenous smRNAs

(A) Autoradiogram of endogenous SSB (red arrow) after immunoprecipitation from UV-crosslinked cells. ^{32}P labeled ribonucleoprotein complexes were treated with either or high concentrations of RNase A digestion prior to separation on SDS-PAGE gel. (B-C) Autoradiograms of immunoprecipitations from cross-linked cells for endogenous hnRNPA1 (A) and hnRNPA0 (B). ^{32}P labeled ribonucleoprotein complexes with either no, low, or high concentrations of RNase A digestion before separating on SDS-PAGE gels.

We next sought to define the identities of the small RNAs bound by hnRNPA1 and SSB. An analysis of tRFs bound in a previously published CLIP-seq study for hnRNPA1 (Huelga et al., 2012) showed the reciprocal RBP-tRF interaction (Fig 4.10). As an abundant RBP, hnRNPA1 has many known roles in regulating gene expression, including as a regulator of splicing and by binding to AU-rich elements (AREs) in 3' UTRs during mRNA turnover and degradation (Geissler et al., 2016; Hamilton et al., 1997; Jean-Philippe et al., 2013).

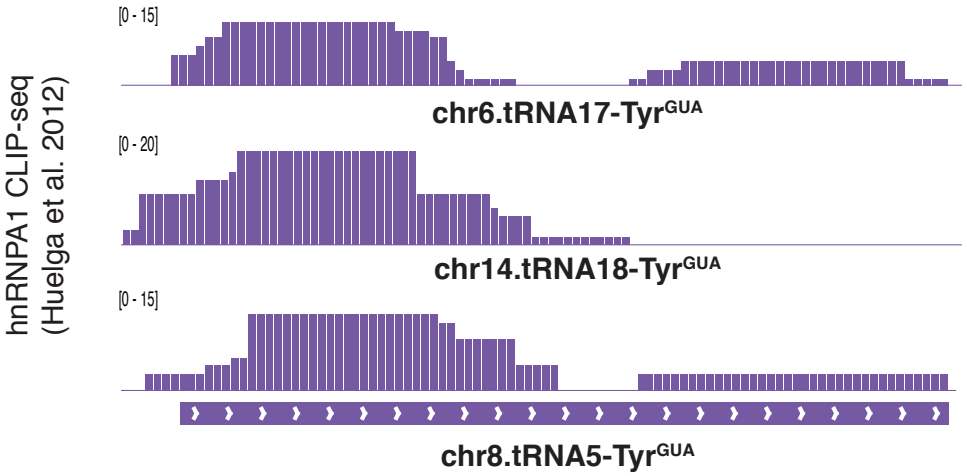

Figure 4.10. Analysis of an hnRNPA1 HITS-CLIP for tRF^{Tyr}_{GUA} binding
IGV plots from an hnRNPA1 HITS-CLIP (Huelga et al., 2012) reveals interactions with the tRF^{Tyr}_{GUA}.

We next conducted HITS-CLIP for endogenous SSB with and without RNase digestion. SSB, also known as La, is a well characterized RNA-binding protein known to bind the nascent 3' ends of Pol III transcripts, including those of full-length pre-tRNAs (Gottlieb and Steitz, 1989; Maraia et al., 1994; Yoo and Wolin, 1997). Beyond its described nuclear roles in Pol III transcript binding, key cytoplasmic functions for SSB have also been reported including regulating translation of certain cellular and viral mRNAs (Costa-Mattioli et al., 2004; Maraia et al., 2017).

Although our HITS-CLIP experiment was designed to enrich for signal from tRFs, we found that consistent with its previously described canonical role in binding Pol III transcripts, alignment and analysis of sequencing reads revealed binding of SSB to the 3'-trailers of pre-tRNAs (Fig 4.10).

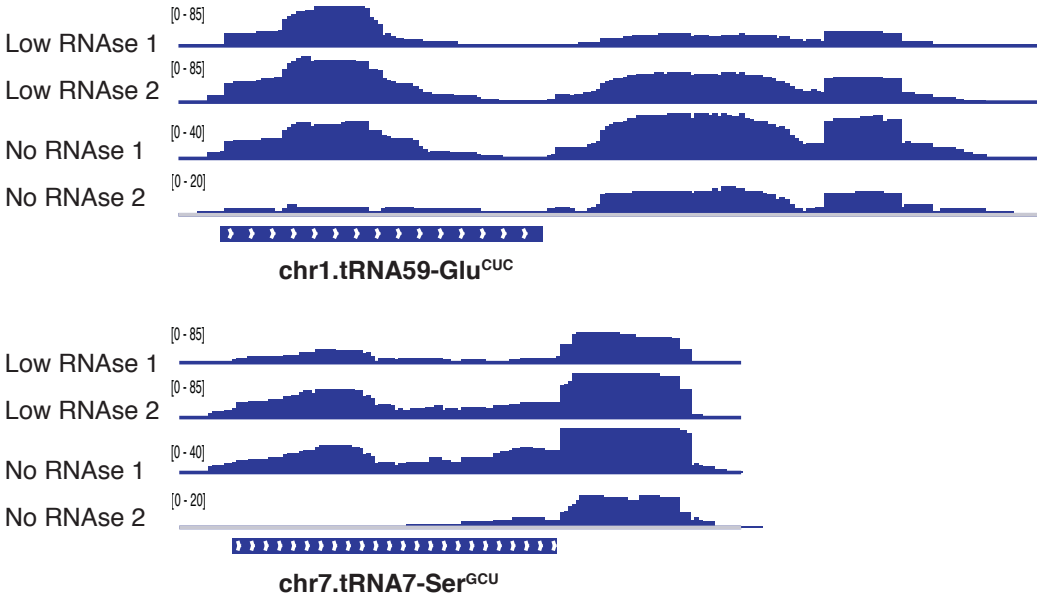

Figure 4.11. SSB HITS-CLIP shows the canonical binding to the 3' end of pre-tRNAs

IGV plots from the SSB HITS-CLIP reveals protein binding to the 3' trailer end of pre-tRNAs arising from distinct tRNA loci.

Importantly, in addition to this previously described binding, we observed previously unreported interactions of SSB with the 5' tRF^{Tyr}_{GUA} arising from multiple distinct loci (Fig 4.11A-B). In experiments with and without RNase, sequencing reads mapping specifically to the tRF^{Tyr}_{GUA} were detected. The abundant number of reads mapping to the 5' regions of $tRNA^{Tyr}_{GUA}$ distinguish these SSB-tRF interactions from the previously described canonical SSB interactions with 3'-trailers of full-length pre-tRNAs. This notion is further supported by our observations of SSB binding to the 5' tRF without 3'-

trailer binding even in the absence of RNase digestion. These observations reveal that tRF$^{Tyr}_{GUA}$ interacts in *trans* with endogenous RBPs in mammalian cells.

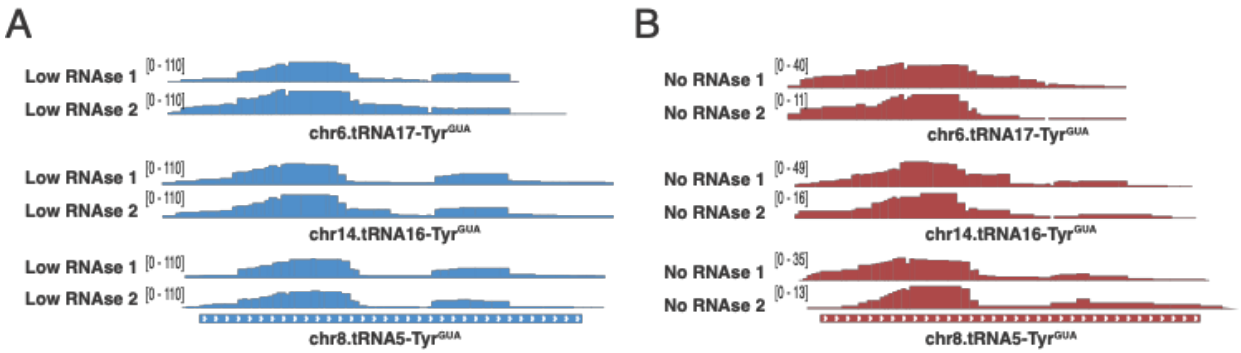

Figure 4.12. SSB HITS-CLIP reveals endogenous tRF$^{Tyr}_{GUA}$ binding
(A) IGV plots representing SSB interacting with the tRF$^{Tyr}_{GUA}$ in samples that were treated with low levels of RNase digestion. SSB bound tRF$^{Tyr}_{GUA}$ reads mapped to multiple loci encoding tRNA$^{Tyr}_{GUA}$. (B) Similar to the IGV plots shown in (A), but depicting SSB interactions with tRF$^{Tyr}_{GUA}$ loci in samples without RNase digestion.

4.5 Functional characterization of tRF$^{Tyr}_{GUA}$

With high confidence between an endogenous tRF$^{Tyr}_{GUA}$-RBP interaction, we looked to determine if the activity of either hnRNPA1 or SSB was regulated through tRF$^{Tyr}_{GUA}$. Following transfection of the tRF$^{Tyr}_{GUA}$ mimetic, we noted no difference in expression of Pol III transcriptional targets, suggesting that the canonical nuclear role

for SSB was unaffected by the presence of the tRF^{Tyr}_{GUA} (Fig 4.12). While SSB is known to localize to both the nucleus and cytoplasm, the distribution of tRF^{Tyr}_{GUA} was unknown.

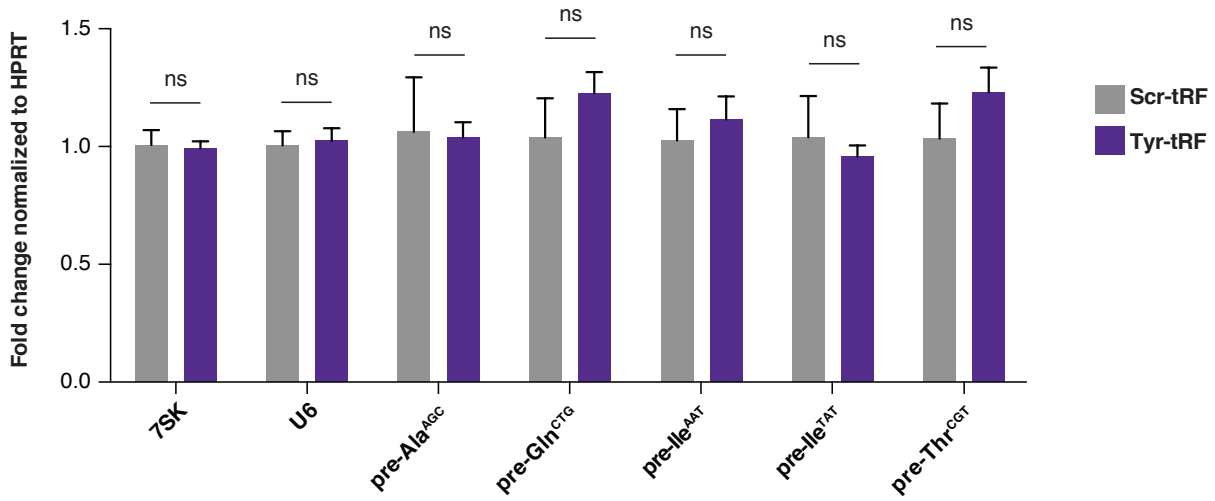

Figure 4.13. Nuclear functions of SSB are unaffected by tRF^{Tyr}_{GUA} transfection

Quantitative RT-PCR expression levels for various Pol III transcribed targets from MCF10A cells transfected with the tRF^{Tyr}_{GUA} mimetic or a scrambled control.

Cytoplasmic and nuclear fractionation of MCF10A cells revealed that the tRF, along with the mature tRNA, were localized almost completely in the cytoplasm (Fig 4.13). Besides any potential sequestering effects, it followed that SSB's nuclear role was unaffected by the tRF. The potential role for regulation of SSB in the cytoplasm is unknown and further study will be required to understand if any functional output from this interaction occurs.

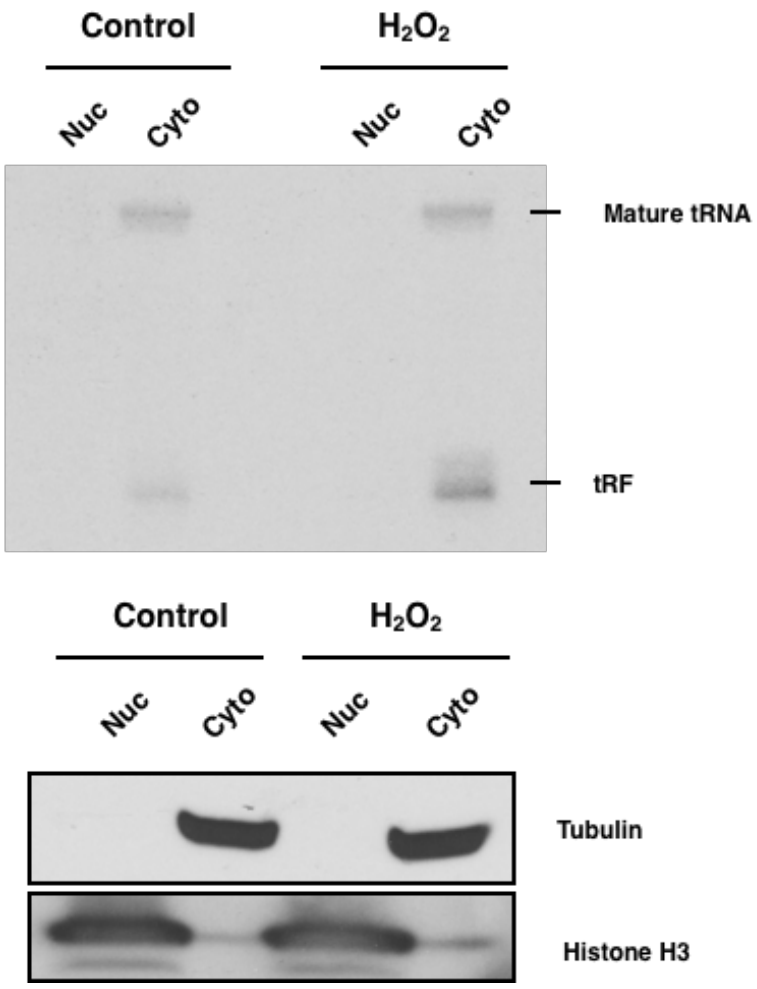

Figure 4.14. Subcellular localization of the tRF^{Tyr}_{GUA}

Nuclear and cytoplasmic fractionation of MCF10A cells reveals that both the mature $tRNA^{Tyr}_{GUA}$ and tRF^{Tyr}_{GUA} are almost completely found in the cytoplasm (top). Western blotting of Tubulin (cytoplasm) and Histone H3 (nucleus) were used as markers for fractionation.

We next sought to determine if the tRF^{Tyr}_{GUA} could regulate the cytoplasmic activity of hnRNPA1. Although hnRNPA1 is best characterized as an RBP that regulates mRNA splicing, we focused on its role in binding to 3' UTRs as the localization of the tRF most likely precluded changes in splicing. Using the 3' UTR targets of hnRNPA1 previously identified by CLIP-seq (Huelga et al., 2012), we looked at hnRNPA1-dependent mRNA stability effects after tRF^{Tyr}_{GUA} overexpression. Following transfection of the tRF^{Tyr}_{GUA} mimetic or a scrambled control in cells with siRNA against hnRNPA1 or a control hairpin, we observed an increase in mRNA stability for hnRNPA1 targets (Fig 4.14A), suggesting that the tRF can compete with the RBP for binding to its endogenous targets. Displacement of hnRNPA1 from it's 3' UTR targets resulted in an increase mRNA stability in an α-amanitin-mediated manner. Consistent with previous findings of hnNRPA1 binding to AREs, an AU-rich motif was significantly enriched in the 3' UTR CLIP tags for hnRNPA1 (Fig 4.14B) (Geissler et al., 2016; Hamilton et al., 1997).

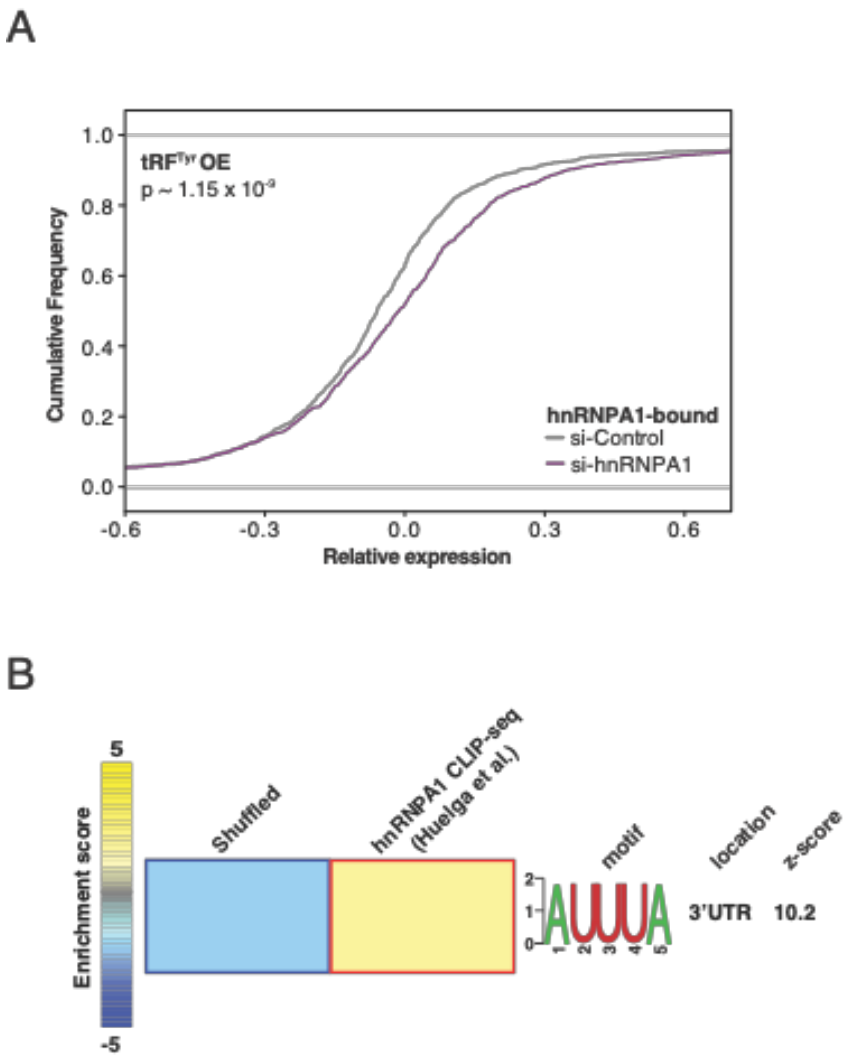

Figure 4.15. tRF$^{Tyr}_{GUA}$ regulates mRNA stability in an hnRNPA1-dependent manner

(A) A cumulative distribution in control and hnRNPA1 knockdown cells of the expression levels for mRNA transcripts with 3' UTR hnRNPA1 CLIP binding (Huelga et al., 2012) . Transfection of the tRF$^{Tyr}_{GUA}$ led to a significant right-shift in the expression level of the 3' UTR bound hnRNPA1 transcripts. Statistical significance was measured using the Kolmogorov-Smirnov test. (B) An AU-rich motif was identified to be significantly enriched in 3' UTR bound hnRNPA1 CLIP targets (Huelga et al., 2012).

GO functional analysis of the 3' UTR targets for hnRNPA1 revealed that cell cycle and DNA damage response genes were significantly enriched and represented the genes stabilized by a displacement of hnRNPA1 by the tRF^{Tyr}_{GUA} (Table 4.1). Our findings describe that stress-induced fragmentation can cause a specific transfer RNA to become depleted, resulting in translational consequences, and also give rise to a tRNA fragment that can interact in *trans* and functionally regulate an RNA-binding protein.

Table 4.1 GO functional analysis of genes regulated by hnRNPA1 in their 3' UTRS

GO terms	Description	Fold Enrichment	p-value
GO:0031572	G2 DNA damage checkpoint	5.36	1.60E-04
GO:0032456	endocytic recycling	4.47	5.03E-04
GO:1902017	regulation of cilium assembly	4.38	3.61E-05
GO:0032205	negative regulation of telomere maintenance	4.23	7.03E-04
GO:0042059	negative regulation of epidermal growth factor receptor signaling pathway	3.88	6.45E-04

4.6 Summary

In this chapter, the characterization of tRF^{Tyr}_{GUA} induction following oxidative stress are further explored. The induction of tRF^{Tyr}_{GUA} is a rapid response but interestingly appears to be in a distinct pathway separate from the effects of $tRNA^{Tyr}_{GUA}$ depletion discussed in chapter 3. Instead, the tRF^{Tyr}_{GUA} that originates from the pre-tRNA acts as a small noncoding RNA that interacts with various RNA binding proteins. Interactions with SSB and hnNRPA1 were both validated by HITS-CLIP and that in a hnRNPA1 dependent manner, can lead to modulations of mRNA stability and gene expression. The subset of genes stabilized by tRF^{Tyr}_{GUA} competitively binding to hnRNPA1 are enriched for DNA damage response and cell cycle regulation, consistent with a necessary reaction to a potent oxidative stress.

CHAPTER 5: Discussion

5.1 The discovery and biological consequences of tRNA fragmentation in response to cellular stress

Aberrant tRNA breakdown products were first detected nearly forty years ago upon analyses of the urine of cancer patients (Gehrke et al., 1979). Since then, tRF induction in response to stress was first characterized in *Tetrahymena* after starvation (Lee and Collins, 2005). Though the functional consequence of this discovery was not elucidated, this finding was an important step to opening a new field in tRNA biology and understanding another level of regulation for gene and protein expression. Subsequent studies found tRNA fragments to be produced in response to numerous different types of stresses, such as heat, hypoxia, and irradiation, in multiple species and domains of life (Fu et al., 2009; Goodarzi et al., 2015; Thompson et al., 2008).

Early studies of specific tRFs in *Saccharomyces cerevisiae* revealed that the given tRNA they were derived from were not impacted upon tRNA fragmentation (Saikia et al., 2012; Thompson and Parker, 2009b). As others found tRFs to be induced following cell stress without modulation of the mature tRNA pool, it was thought that fragmentation left the mature tRNA population relatively unchanged (Kirchner and Ignatova, 2015). However, a more thorough and comprehensive analysis was required before this conclusion could be determined.

The advent of numerous methods that enabled profiling of tRNAs revealed widespread alterations in tRNA expression allowed us to tackle this question using a combination of both novel and classic molecular biology assays (Cozen et al., 2015; Dittmar et al., 2006; Gogakos et al., 2017; Goodarzi et al., 2016; Zheng et al., 2015). Genomic copy number gains at tRNA loci have been shown to account for enhanced expression of specific tRNAs that functionally drive cancer progression (Goodarzi et al., 2016; Truitt and Ruggero, 2016). This has raised the question of whether in the absence of genomic instability, endogenous pathways exist for physiological modulation of tRNA levels with functional consequences. Our observations reveal that in non-malignant epithelial cells, there exists an oxidative stress response pathway that represses growth upon selective tRNA depletion.

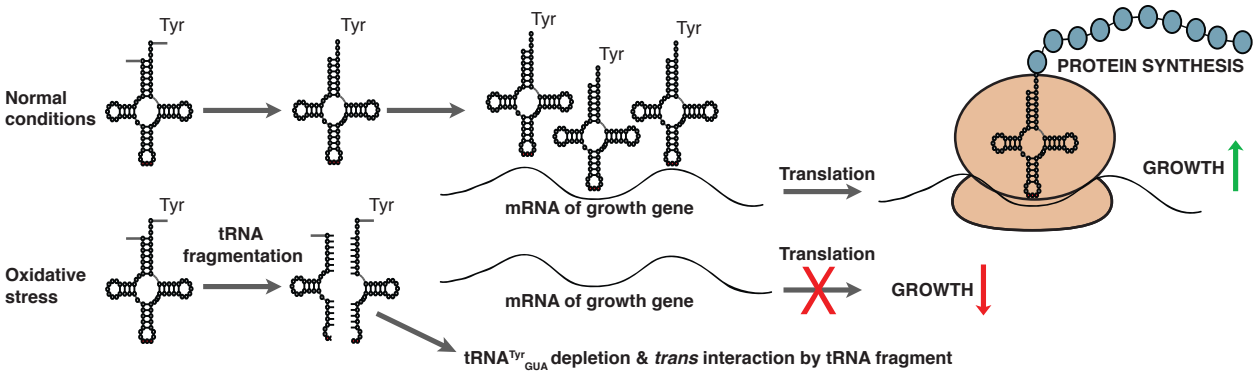

Illustration 5.1 Model of tRNA$^{Tyr}_{GUA}$-dependent gene regulatory response to oxidative stress.

A schematic of our findings describing a tRNA fragmentation response to oxidative stress. Fragmentation of pre-tRNA$^{Tyr}_{GUA}$ results in a codon dependent based repression of translation and growth as well as affecting gene expression through interactions between the tRF$^{Tyr}_{GUA}$ and hnRNPA1.

5.2 Elucidating the downstream effects of tRNA depletion

With evidence of $tRNA^{Tyr}_{GUA}$ depletion as a delayed response to oxidative stress, we sought to identify the functional outcome of this modulation. Our work identified that this $tRNA^{Tyr}_{GUA}$ depletion led to codon-dependent translational repression of a subset of growth promoting proteins. This tRNA and protein depletion response likely cooperates with other cellular oxidative response pathways (Martindale and Holbrook, 2002) to act as a robust suppressor of cell growth. Despite our observations on the negative impact on translation with a decrease in tRNA abundance, the exact biological mechanisms that govern this response is still not completely understood.

The current hypothesis is that when the translating ribosome comes across a codon where the cognate tRNA is non-optimal or lowly abundant, the ribosome slows and stalls. This stalled ribosome then is recognized by many factors, including Dhh1p in yeast (Radhakrishnan et al., 2016), to stimulate mRNA degradation. Decreased translation from this stalled ribosome can be detected through increased codon occupancy in the ribosome (Wu et al., 2019). This is most likely, much like many models in biology, an oversimplified model of what is actually occurring in the ribosome as many questions remained unanswered. Is translation for each transcript identical or similar enough to expect the majority of transcripts found in the cell to respond in the same way? How does ribosome stalling and decreased translation affect the mRNA and

growing polypeptide chain? What compensatory responses exist in the case of tRNA depletion?

Many of the experiments looking at global translation show that that mRNAs and protein expression can both be decreased as well as increased. Even in our own data with $tRNA^{Tyr}_{GUA}$ depletion, we noted a significant overlap of genes with high tyrosine content and decreased translational efficiency, but could find numerous examples of transcripts or proteins that contained tyrosines to be increased in expression. Many *in vitro* techniques used to validate our ideas use reporter constructs for one or at most, a few of the most highly sensitive genes. While this is necessary for initial proof of principle, it fails to show how certain mRNAs or proteins containing codons read by a lowly abundant tRNA may be immune to decreased expression or may even be increased in expression. One hypothesis to explain this is that translation of one transcript may be quite differently regulated when compared to another. There may be unknown factors and regulators of translation, like Dhh1p, that affect both mRNA stability and translation. Future experiments could include immunoprecipitation of ribosome subunits in both stressed and unstressed cells to identify other protein factors that might influence translation. Similarly, with quality endogenous or fluorescent reporters that reflect changes in translation, siRNA or CRISPR screens could also be used to identify these regulators of translation. In a system like ours, one could deplete $tRNA^{Tyr}_{GUA}$, expecting USP3 to become decreased as well, and look for modulations in the level of this reporter following an overexpression or knockout screen. Although many false positives in the form of transcriptional regulators might be isolated as well, the

overlap of multiple reporters might be able to offer both further insight and higher confidence targets.

While our work has interrogated the consequences of $tRNA^{Tyr}_{GUA}$ depletion, future work is needed to determine the impact, if any, of depletions of other tRNAs that were observed to generate fragments and also become depleted. Two such examples are $tRNA^{Leu}_{UAA}$ and $tRNA^{Leu}_{CAG}$. Interestingly, although there exist six isoacceptor tRNAs for leucine, we only observed significant concomitant tRF induction and tRNA depletion for these two isoacceptors, suggesting potential tRNA fragmentation selectivity amongst the isoacceptors for a given amino acid, with potential for codon-biased translational consequences.

Previous studies have assessed the relationship between global tRNA modulations and effects on translation in *E. coli* (Wohlgemuth et al., 2013; Zhong et al., 2015). Consistent with our findings, the studies in *E. coli* have revealed that protein translation can be impacted by cellular tRNA availability. While oxidative stress has been observed to repress global tRNA levels in *E. coli* (Zhong et al., 2015) and *S. cerevisaie* (Torrent et al., 2018), our results reveal that in mammalian cells, there is a selective tRNA and codon-dependent response to oxidative stress. Differences in stress response between mammalian cells and unicellular organisms suggests that higher organisms may have evolved mechanisms for selective tRNA modulation in response to a key cellular stress. Future studies are warranted to investigate these possibilities. While we do not yet know the mechanistic basis for this selectivity, we speculate that the tRNAs that become modulated upon oxidative stress may be targeted based off

abundance, modifications present, or that various steps in tRNA processing might be targets of regulation.

5.3 Identifying ribonucleases that cleave tRNAs to generate tRFs

Further investigation into tRNA processing may elucidate additional mechanisms by which cells post-transcriptionally regulate protein expression. Though our data indicates that tRNA splicing is not the main source of tRF induction, we cannot rule out the possibility that other unknown RNases might also have a role in the tRNA splicing complex. If the known tRNA splicing complex is involved, a genetic deletion of TSEN2 might be necessary to completely blunt tRF induction upon oxidative stress. A complete knockout may be necessary to be sure of excluding ANG as an RNase that also induces the tRF^{Tyr}_{GUA} upon oxidative stress. An alternative experiment to completely eliminate ANG could be to show that this RNase has no activity or binding to the pre-tRNA and only cleaves at the anticodon loop of mature tRNAs.

Identifying RNases that cleave tRNAs remains a challenge in the field. Similar to RNA binding proteins promiscuously binding to many different types of RNA, RNases often recognize common elements found in many different RNA species. As a result, it is a challenge to both identify an RNase that can cleave tRNAs but does so endogenously and is not an artifact of the *in vitro* conditions. Furthermore, the relatively quick timeframe in which tRNAs become fragmented most likely impedes identification of potential RNases by analyzing gene expression profiles following stress. In the case

of Rny1p, the protein is always present in cells but sequestered away to prevent fragmentation until the cell experiences stress (Thompson and Parker, 2009a). If localization represents the main difference between seeing tRFs and not, then it becomes all the more challenging to identify RNases that show no difference at the transcript or protein level.

Instead, future experiments might need to focus on different approaches. One potential method could be to look at functional consequences for downstream factors, such as USP3, SCD, or EPCAM. Potentially fusing USP3 to a fluorophore instead of a Myc-tag and combining flow cytometry with CRISPR screens could yield new prospects for RNases that cleave the pre-tRNA$^{Tyr}_{GUA}$. Alternatively, with the sequence of both tRF and pre-tRNA known, one potential experiment could create a synthetic pre-tRNA that has a modified base that is resistant to cleavage. This bait could be used to trap potential RNases that could be later identified by mass spectrometry. As this method is only possible by knowing the site of cleavage, it is only applicable in certain cases. With the ease of sequencing and newer methods for sequencing tRNAs becoming available, exact sites of cleavage may become more characterized to allow using a synthetic bait for other tRFs. Despite the increase in resolution from sequencing, this potential method also has experimental caveats such as the synthetic pre-tRNA may not resemble the endogenous one due to a lack of modifications, resulting in a lack of interaction with the target ribonuclease. Similarly, it might also be possible that the modified nucleotides themselves prevent binding to the RNase as it prevents recognition by the enzyme.

Despite these obstacles, new RNases will surely be identified and validated to create tRFs in the future. It will undoubtedly be interesting to learn how these ribonucleases can become active within minutes of cellular stress and how they maintain specificity for not only specific tRNAs, but also for locations on a given tRNA. Fragments where tRNAs are cut in the D-loop, anticodon loop, and T-loop have all been reported but it remains unknown how a given location on a tRNA is chosen for cleavage over another. Moreover, tRFs have been previously implicated in regulating cancer (Goodarzi et al., 2015) and dysregulated tRNA splicing, resulting in persistent introns, have also been linked with neuronal degeneration (Karaca et al., 2014; Schaffer et al., 2014). Identification of ribonucleases that give rise to tRFs involved with human diseases might offer another avenue for therapeutic interventions.

5.4 Understanding the functional effects of tRFs

While our understanding of the mechanisms behind tRNA cleavage is poorly characterized, many groups have found that these tRFs may have functional roles in the cell. Previous studies have shown tRFs can regulate mRNA stability, translation initiation, rRNA biogenesis, as well as being involved with other roles (Goodarzi et al., 2015; Kim et al., 2017; Yamasaki et al., 2009). As a relatively novel species of RNA, tRFs represent a highly abundant and malleable class of noncoding RNA.

In this study, we have implicated hnRNPA1 and SSB/La as RNA binding proteins that directly interact with tRF^{Tyr}_{GUA}. SSB/La has numerous cellular functions, perhaps

chief among them being pre-tRNA processing (Gottlieb and Steitz, 1989; Wolin and Cedervall, 2002). While future work is necessary to define the potential regulatory role of this interaction, the interaction of a stress-induced tRNA fragment with a central regulator of physiological tRNA processing suggests a potential regulatory feedback loop that may impact tRNA maturation upon stress induction. Interestingly, as the tRF^{Tyr}_{GUA} is predominantly cytoplasmic, we currently do not see a difference in nuclear Pol III transcripts known to bind to SSB. Future work could take a deeper look at the SSB bound RNAs in the nuclear and cytoplasmic fraction to identify if this RBP-tRF interaction occurs exclusively in the cytoplasm or if it can be detected in the nucleus as well. Experiments interrogating the known roles of SSB in the cytoplasm also require further study as SSB is known to regulate translation of various mRNA targets, though many arise from viral IRES mRNAs (Wolin and Cedervall, 2002). However, as tRFs have been detected in response to viral infection (Deng et al., 2015; Zhou et al., 2017), it seems possible that a response can be seen through tRFs and tRNAs as they represent ancient and fundamental aspects of cell biology.

Similar to SSB, hnRNPA1 has multiple known roles in regulating RNAs (Jean-Philippe et al., 2013). It has been shown to bind to AU-rich regions in 3' UTRs to regulate mRNA degradation (Jean-Philippe et al., 2013), a motif seen in a new analysis of 3' UTR targets from a previously published hnRNPA1 CLIP-seq (Huelga et al., 2012). Our data suggests that the tRF^{Tyr}_{GUA} competes with these 3' UTRs for binding to hnRNPA1 and as a consequence, stabilizes these endogenous mRNA targets. Perhaps unsurprisingly, these now stabilized mRNAs are significantly enriched in genes that

regulate G2/M checkpoints and DNA damage response, key factors in protecting the cell from the damage reactive oxygen species can have on DNA. When looking at the response to oxidative stress as a whole, this hnRNPA1 effect fits in well as an immediate response. As the tRF is immediately induced, the tRF competes with endogenous binding partners of hnRNPA1, thereby stabilizing genes involved in DNA damage and cell cycle regulation. A delayed reduction of the tRNA is then observed leading to repression of cell growth meaning that the total response to oxidative stress both increases a response to maintain genomic integrity and decrease energy expenditure on translation and cell division.

Our study explores a divergent response to oxidative stress that originates from an unexpected single tRNA precursor. However, this work offers plenty of questions for future study. Beyond hnRNPA1 and SSB, tRF^{Tyr}_{GUA} likely interacts with other RBPs and it would be worth investigating other regulatory functions for this tRF. We have only followed up on a few of the top hits from mass spectrometry but many other remain uncharacterized. Likewise, oxidative stress yielded numerous changes at both the tRNA and tRF level. How these other affected molecules contribute to this response will surely increase our understanding of how tRNAs and tRFs are involved in a regulating the cellular landscape beyond as an adaptor molecule used to convert mRNAs into proteins.

Lastly, it will be particularly interesting to understand how different stresses may induce different tRFs. Future work could compare the similarities and differences between these networks of noncoding RNA that are induced and the functional outputs

when interacting with other factors. Even different tissue types may respond differently to the same stress as the metabolic and tRNA profiles can vary greatly. With further investment and advances in technology to quantify tRNAs and their derived fragments, the roles of these noncoding RNAs will offer greater insight into how the cell operates in both basal and stressed conditions.

Materials and methods

Cell culture

MCF10A cells were cultured in DMEM/F12 media supplemented with 5% horse serum and final concentrations of 20 ng/ml of EGF, 0.5 mg/ml of hydrocortisone, 100 ng/ml of cholera toxin, and 10 μg/ml of insulin. HBEC30 cells were cultured in keratinocyte-SFM media with the included supplements of BPE and EGF. All cell lines were STR tested and routinely tested for mycoplasma contamination. To induce oxidative stress, cells were incubated with 200μM H_2O_2 or 50μM of menadione (Sigma) dissolved in DMSO in their respective medias for the time specified in each experiment. RNA was then isolated by TRIzol and isopropanol precipitation as described below.

Stable cell line generation

Lentivirus was produced in 293T cells grown in 10 cm plates. 3 μg of each packaging vector (pRSV-Rev, pCMV-VSVG-G, and pCgpV) were transfected with 9 μg of the appropriate hairpin in a pLKO-backbone vector using 30 μl of Lipofectamine 2000 (Invitrogen). After 24 hours, the media was replaced with fresh media and virus-containing supernatant was harvested 48 hours after transfection. The supernatant was filtered through a 0.45 μm filter before 2 ml of virus was used to transduce MCF10A cells plated in 6-well plates with 8 μg/ml of polybrene. Media was changed after 24 hours and antibiotic selection with 1 μg/ml of puromycin was started 48 hours after virus transduction. Targeted sequences used for stable RNAi cell lines were:

TTATGCCACAGTCCTTATAAT (YARS sh2), GTTCATCAAAGGCACTGATTA (YARS sh3), and TGGTAGAGCGGAGGACTGTAGA ($tRNA^{Tyr}_{GUA}$). Cells were selected for 3-5 days with a population of non-transduced cells as a control. Knockdown of mRNA and protein were validated by qRT-PCR and western blot, respectively, while knockdown of tRNA was validated by northern blot.

RNA isolation and purification

RNA was extracted from cells using TRIzol and isopropanol precipitation at -20°C overnight. After centrifugation at max speed (~21,000 x *g*) in a refrigerated tabletop centrifuge, the RNA pellet was washed twice with ice-cold 75% EtOH before being resuspended in RNase free water or TE-buffer.

Northern blotting

Purified RNA was run on a 10% Urea-PAGE gel before being transferred onto a nylon membrane and UV crosslinked (240 mJ/cm^2). The membrane was pre-hybridized in UltraHyb-Oligo buffer (Ambion) at 42°C. DNA oligos were radiolabeled with [γ-^{32}P]ATP using T4 PNK (NEB) and further purified by G-25/G-50 columns before incubating with the blot overnight. After hybridization, the blot was washed twice with SSC and SDS buffers before being developed. Probes that were ^{32}P labeled and used for detection were: ACAGTCCTCCGCTCTACCAGCTGA ($tRNA^{Tyr}_{GUA}$), CAGCGCCTTAGACCGCTCGGCCA ($tRNA^{Leu}_{HAG}$), AACGCAGAGTACTAACCACTATACG ($tRNA^{His}_{GUG)}$,

GCGCCGAATCCTAACCACTAGACCA ($tRNA^{Glu}_{YUC}$), CACGAATTTGCGTGTCATCCTT (U6), and CAAATTATGCAGTCGAGTTTCCCACATTTG (U1). Quantification was done using FIJI (ImageJ) where the intensity of each band over background was measured and normalized to U6 levels.

Quantitative LC-MS/MS proteomic profiling

For label-free quantitation analysis of protein levels by mass spectrometry, $tRNA^{Tyr}_{GUA}$-depleted and YARS-depleted cells were compared control hairpin expressing cells. For each set of samples, 50ug of lysate (n=3 per condition) was ice-cold acetone precipitated. Precipitates were dissolved in 50uL 8M Urea/0.1M ammonium bicarbonate/10mM DTT. After 45 minutes of incubation at room temperature, reduced cysteines were alkylated with iodoacetamide (Sigma) in the dark for 45 minutes. Volumes were diluted 2-fold and proteins were digested overnight with 1 μg Lysyl Endopeptidase (Wako). Prior to trypsinization (1ug) (Promega), the samples were diluted an additional 2-fold (0.1 M ammonium bicarbonate). After 8h, the digestions were halted by the addition of neat TFA (Sigma) and then peptides were desalted and concentrated using stage tips.

Peptides were separated using a direct-loading setup with a 50cm EasySprayer C_{18} column (ES80, Thermo). Peptides were eluted using a gradient increasing from 2% B/98% A to 45% B/55% A (A: 0.1% formic acid, B: 80% acetonitrile/0.1% formic acid) in 220 minutes. The gradient was delivered at 300nL/min (Easy 1200, Thermofisher). The

mass spectrometer (Fusion Lumos, Thermo Fisher) was operated in High/High mode with MS and MS/MS mass resolution being 120,000 and 30,000, respectively. For MS/MS, Automatic Gain Control was set to 1e5 with a maximum injection time of 54 ms. MS-data were queried against Uniprot's Human Complete Proteome (70,246 sequences, March 2016) using MaxQuant v1.6.0.13. Oxidized methionine and protein N-terminal acetylation were allowed as variable modifications and up to 2 missed cleavages were allowed. Proteins were quantitated using MaxQuant's 'Label Free Quantitation' (LFQ) feature and signals were required in minimum 2-of-3 replicates for at least one condition (4,753 proteins quantitated). Missing LFQ values where imputed. All data analysis was carried out using Perseus v1.6.0.7.

Western blotting

Cells were lysed in ice-cold RIPA buffer containing a protease inhibitor cocktail (Roche) before cellular debris was cleared by centrifugation at max speed in a refrigerated tabletop centrifuge. Samples were heated with LDS buffer and reducing agent before running on an SDS-PAGE gel and transferred onto a PVDF membrane (Bio-Rad). The membranes were blocked and then probed using target-specific antibodies. Chemiluminescent signal was detected by HRP-conjugated secondary antibodies, ECL western blotting substrate (Pierce), and the SRX-101A (Konica Minolta) developer according to manufacturer's instructions. Membranes were stripped (Restore western blot stripping buffer, Pierce), blocked, re-probed, and re-developed if necessary.

Table M.1 List of antibodies used

Protein	Source	Product	RRID	Dilution
EPCAM	Proteintech	21050-1-AP	AB_10693684	1:1000
hnRNPA0	Bethyl Laboratories	A303-941A	AB_2620290	1:1000
hnRNPA1	Santa Cruz	sc-32301	AB_627729	1:1000
Luciferase	Proteintech	27986-1-AP	AB_2750646	1:1000
Myc-tag	Cell Signaling	2276S	AB_331783	1:1000
SCD	Proteintech	23393-1-AP	AB_2744674	1:1000
SSB	MBL	RN074PW	AB_11124309	1:1000
USP3	Proteintech	12490-1-AP	AB_10639042	1:1000
YARS	Abcam	ab150429	AB_2744675	1:1000
alpha-Tubulin	Cell Signaling	2144	AB_2210548	1:2000
Lamin A/C	Santa Cruz	sc-376248	AB_10991536	1:2000
HSC70	Santa Cruz	sc-7298	AB_627761	1:2000

Quantitative western blotting

To compare protein expression levels by western blot, the Odyssey® quantitative western blotting system (LI-COR) was used. This method is identical to western blotting except membranes were blocked in Odyssey® blocking buffer (PBS) and the secondary antibody used was a species-specific fluorescent IRDye®. Membranes were then imaged using the Odyssey® Sa Infrared Imaging System at the Rockefeller University Center for High Throughput Screening. Image quantification was done using Image Studio™ Lite and an unpaired t-test was used to determine statistical significance.

Codon reporter assays

A Myc-tagged construct was synthesized by Genewiz and cloned into the psiCHECK2 vector (Promega), replacing the synthetic Renilla Luciferase gene. A 6x-glycine linker was placed between the Myc-tag and the gene. The constructs included a wild-type USP3 or a USP3 gene with a set of 5 tyrosines mutated to alanines. Multiple mutant constructs were cloned but only those with high levels of expression were chosen for testing. MCF10A cells were seeded to be 70% confluent in a 6 cm plate the next morning. Cells were exposed to 200μM H_2O_2 or a control for one hour before being transfected with the reporters using Lipofectamine 3000 (Invitrogen). Cells were lysed and compared through quantitative western blotting 24 hours post H_2O_2 treatment.

Quantitative RT-PCR

To measure mRNA transcript levels, RNA was converted to cDNA (SuperScript III, Life Technologies) followed by Fast SYBR™ Green quantification (Life Technologies) according to manufacturer's instructions. Expression levels of mRNA were performed with either an ABI Prism 7900HT Real-Time PCR System (Applied Biosystems) or a QuantStudio 5 Real-Time PCR System (Applied Biosystems).

Table M.2 Sequences of qRT-PCR primers used

Gene	Forward primer (5'-3')	Reverse primer (5'-3')
ANG	CTGGGCGTTTTGTTGTTGGTC	GGTTTGGCATCATAGTGCTGG
CLP1	GGAGTTGTTGACTGGCATGG	CCGCTCAGTTGCACAGAAC
EPCAM	AATCGTCAATGCCAGTGTACTT	TCTCATCGCAGTCAGGATCATAA
HPRT	GACCAGTCAACAGGGGACAT	CCTGACCAAGGAAAGCAAAG
SCD	TCTAGCTCCTATACCACCACCA	TCGTCTCCAACTTATCTCCTCC
TSEN2	ATGCGGAGGACATTGAGCAG	CGGTTTCGTGTAATCCTTGAGG
USP3	CAAGCTGGGACTGGTACAGAA	GCAGTGGTGCTTCCATTTACTT
YARS	CTGCACCTTATCACCCGGAAC	TCCGCAAACAGAATTGTTACCT

Small RNA sequencing

MCF10A cells were seeded at 50% confluency in duplicate into 10 cm plates. The next day, cells were exposed to 200μM H_2O_2 for one hour before harvesting for RNA purification. Small RNA was purified using the microRNA purification kit (Norgen Biotek Corp) according to manufacturer's instructions. To identify the tRF^{Tyr}_{GUA} from the pre-$tRNA^{Tyr}_{GUA}$, RNA was gel extracted between 40-50nt on a TBE-Urea PAGE gel. The RNA was then treated with polyphosphatase (Lucigen) before acid phenol chloroform extraction and RNA precipitation. Small RNA sequencing was performed using the NEXTflex® Small RNA Sequencing Kit v3 (BiooScientific). Different samples were barcoded before being sequenced on the HiSeq 2000 Illumina sequencer. For computational analysis, fastq files were aligned to hg19 using bowtie2, and reads were

further sorted, indexed, and counts were generated with samtools. Raw counts were imported into RStudio V1.1.383 and differential analysis was performed using DESeq2.

Transient overexpression of $tRNA^{Tyr}_{GUA}$

Overexpression constructs for $tRNA^{Tyr}_{GUA}$ were made as previously reported by (Mattijssen et al., 2017) Briefly, 3 copies per plasmid of $tRNA^{Tyr}_{GUA}$ were synthesized by Genewiz into the pUC57-KAN vector. Each copy had 150nt upstream and 90nt downstream genome sequences included but did not include the intron sequence. This vector or an empty pUC57-KAN vector were transiently transfected using Lipofectamine 3000 (Invitrogen).

RNA stability of hnNRPA1 bound transcripts

950,000 MCF10A cells were reverse transfected with a control siRNA or siRNA against hnRNPA1 with either a tRF^{Tyr}_{GUA} mimetic or a scrambled mimetic using Lipofectamine RNAimax (Invitrogen). After 48 hours, half of the samples were treated with α-amanitin (10mg/ml, Sigma) and incubated for 8 hours while the other half was taken as the 0 hour time point. RNA was extracted using TRIzol and RNA-seq libraries were prepared using QuantSeq 3' mRNA-seq kit (Lexogen) following the manufacturer's instructions.

Cell growth assays

300,000 or 400,000 cells were seeded into two 6-well plates. Cells were trypsinized and viable cells were counted using a trypan blue and a hemocytometer on days 1 and 3

after seeding. Each experiment included three technical triplicates and was repeated three times. Two-way ANOVA was used to test for significance.

For growth assays with siRNA-mediated gene knockdown, cells were reverse transfected with siRNA (IDT) and Lipofectamine RNAimax (Invitrogen) so that they would be 70-80% confluent in a 10 cm plate. The following day, cells were seeded at a density of 200,000 cells per 6-well plate and counted on days 1 and 3 after seeding into 6-well plates. As before, two-way ANOVA was used to test for significance.

Cell viability assays

MCF10A cells were seeded into 6-well plates and treated with 200μM H_2O_2 for one hour. This media was retained while cells were trypsinized and then resuspended in the previous media that would contain any cells that had died prior to trypsinization. Cell viability was measured using trypan blue exclusion and a hemocytometer. Viability was determined by (Total number of cells counted – Number of blue (nonviable) cells) / Total number of cells counted. Each experiment included three technical triplicates and was repeated twice. An unpaired *t*-test was used to test for significance.

Transfer RNA profiling

MCF10A cells were cultured in duplicates to be 50% confluent in 10 cm plates. Cells were then exposed to 200μM H_2O_2 for 8 hours or 24 hours before RNA was isolated using the mirVana miRNA isolation kit. Transfer RNA profiling was done as described by (Goodarzi et al., 2016). Briefly, biotinylated probe-pairs against nuclear encoded tRNAs were designed to hybridize to each half of the tRNA. A nick at the anticodon end of the DNA-RNA hybrid was filled using T4 DNA ligase and SplintR ligase (NEB). MyOne-C1 Streptavidin Dynabeads (Invitrogen) were used to purify the DNA-RNA hybrids and ligated probes were eluted following RNase H and RNase A incubation. Eluted probes were PCR amplified and high-throughput sequenced.

For computational analysis, fastq files were aligned to tRNA probe sequences using bowtie2, and reads were further sorted, indexed, and counts were generated with samtools. Raw counts were imported into R V3.4.1 and normalized with EdgeR. Linear regression tests were used to assess tRNAs that were significantly depleted at 8 and 24 hour conditions relative to control conditions.

Whole-genome ribosomal occupancy profiling

This procedure was conducted as described by (McGlincy and Ingolia, 2017). Briefly, cells were washed and flash frozen with liquid N_2 before being lysed with lysis buffer containing cycloheximide (Alfa Aesar). Lysate was digested with RNase I (Lucigen) before ribosomes were isolated through ultracentrifugation through a sucrose cushion.

The ribosome pellet was resuspended in a solubilization buffer containing 0.5% SDS and 1mM EDTA and TRIzol before RNA was extracted using the Direct-zol kit (Zymo Research). RNA was separated on a 15% TBE-Urea gel before RNA between 17nt and 34nt were gel extracted. Barcoded pre-adenylated linkers were ligated using T4 RNA ligase 2 truncated K227Q (NEB) and rRNA was depleted using the Ribo-Zero gold kit (Illumina) according to the manufacturer's protocol. RNA was converted to cDNA using SuperScript III (Life Technologies) and the RT product was circularized by CircLigase II (Epicentre). A PCR library was amplified and sequenced using Illumina Nextseq 500 at the Rockefeller University Genomics Center.

For the ribosome footprinting data, reads were first subjected to linker removal and quality trimming (cutadapt v1.17). The reads were then distributed among the samples based on their assigned barcodes using fastx_barcode_splitter (using --eol and --mismatches 1). The reads were then collapsed and UMIs were extracted in two steps (2 at the 5' end and 5 at the 3' end) using UMI Tools. The reads were then aligned against a reference database of rRNAs and tRNAs as to remove contaminants (using bowtie 2.3.4.1). STAR was then used to align the remaining reads to the human transcriptome (build hg38). PCR duplicates were then removed using UMI Tools. Xtail (Xiao et al., 2016) was used to count RPFs, estimate translation efficiency, and perform statistical comparisons. For RNA-seq data analysis, reads were first subjected to quality trimming and adapter removal. STAR (v2.5.2a) was used to align the reads to the human

transcriptome (hg38). The number of reads mapping to each gene was counted using htseq-count.

Analysis of translational efficiency from ribosome profiling

The logTER (log2 of translation efficiency ratio) between shTyr and shControl samples calculated by Xtail showed a substantial and significant GC bias. As such, prior to further analysis, we first corrected the logTER values by fitting a linear model based on GC content of each genes as the co-variate. We then used the GC-independent residual values for further analysis. We asked whether stratifying genes based on their Tyr content is informative of corrected TER measurements. For this, we performed a t-test between two groups defined by the Tyr content of the 75^{th} percentile. At this threshold, we observed a significantly lower TE for in the shTyr samples ($P<0.0002$). To perform a confirmatory analysis, we also performed a gene-set analysis using our iPAGE platform (Goodarzi et al., 2009). This analysis also revealed a significant enrichment of genes with high Tyr content (same threshold as above) among those in the bottom tertile of the GC-corrected logTER values.

Using the tRF^{Tyr}_{GUA} mimetic to identify interacting proteins

A 5' biotinylated 37-nucleotide tRF^{Tyr}_{GUA} mimetic (CCUUCGAUAGCUCAGCTGGUAGAGCGGAGGACUGUAG) and a control oligo (GAGACCAGGGUACGCAAUCGAGUUGUUGGGCACUCUG) that was a scrambled version of the tRF^{Tyr}_{GUA} were synthesized (IDT). Each mimetic was incubated at 4°C

with equal amounts of MCF10A cell lysate containing protease inhibitor that had been pre-cleared for debris and by the control oligo. Proteins that bound to our mimetic were co-precipitated by MyOne-C1 Streptavidin Dynabeads (Invitrogen) and washed twice with a low salt wash buffer (50mM Tris-HCl pH 7.5, 150mM NaCl) and twice with a high salt wash buffer (50mM Tris-HCl pH 7.5, 400mM NaCl) before being submitted to the Rockefeller University Proteomics Resource Center.

SSB HITS-CLIP with and without RNase

HITS-CLIP for endogenous SSB was done as described by (Licatalosi et al., 2008) with the modifications previously used for YBX1 small RNA CLIP (Goodarzi et al., 2015). MDA-MB-231 cells were UV-crosslinked at 400 mJ/cm^2 before cell lysis. Samples with and without RNase treatment were immunoprecipitated with an anti-SSB antibody (MBL, RN074PW) for protein-RNA complexes. Polyphosphatase (Lucigen) was incubated with smRNA samples before ligation and PCR amplification with primers described by (Goodarzi et al., 2015). Constructed libraries were sequenced on the Illumina HiSeq2000 at the Rockefeller University Genomics Center.

The CTK package (Shah et al., 2017) was used to analyze the SSB HITS-CLIP data. First, reads were distributed to individual samples based on the integrated 4nt barcodes. The reads were then collapsed, trimmed, and aligned to the human genome (hg19) using bwa (0.7.17-r1188; -n 0.06 -q 20). The CTK toolkit was then used parse the alignments, remove PCR duplicates, and call mutations in reads. The results from

biological replicates were then combined and the CIMS tool (CTK) was used to call peaks (FDR<0.1).

References

Ashburner, M., Ball, C.A., Blake, J.A., Botstein, D., Butler, H., Cherry, J.M., Davis, A.P., Dolinski, K., Dwight, S.S., Eppig, J.T.*, et al.* (2000). Gene ontology: tool for the unification of biology. The Gene Ontology Consortium. Nat Genet *25*, 25-29.

Bjork, G.R., Wikstrom, P.M., and Bystrom, A.S. (1989). Prevention of translational frameshifting by the modified nucleoside 1-methylguanosine. Science *244*, 986-989.

Cerini, C., Kerjan, P., Astier, M., Gratecos, D., Mirande, M., and Semeriva, M. (1991). A component of the multisynthetase complex is a multifunctional aminoacyl-tRNA synthetase. EMBO J *10*, 4267-4277.

Chen, Q., Yan, M., Cao, Z., Li, X., Zhang, Y., Shi, J., Feng, G.H., Peng, H., Zhang, X., Zhang, Y.*, et al.* (2016). Sperm tsRNAs contribute to intergenerational inheritance of an acquired metabolic disorder. Science *351*, 397-400.

Chi, S.W., Zang, J.B., Mele, A., and Darnell, R.B. (2009). Argonaute HITS-CLIP decodes microRNA-mRNA interaction maps. Nature *460*, 479-486.

Cole, C., Sobala, A., Lu, C., Thatcher, S.R., Bowman, A., Brown, J.W., Green, P.J., Barton, G.J., and Hutvagner, G. (2009). Filtering of deep sequencing data reveals the existence of abundant Dicer-dependent small RNAs derived from tRNAs. RNA *15*, 2147-2160.

Costa-Mattioli, M., Svitkin, Y., and Sonenberg, N. (2004). La autoantigen is necessary for optimal function of the poliovirus and hepatitis C virus internal ribosome entry site in vivo and in vitro. Mol Cell Biol *24*, 6861-6870.

Couvillion, M.T., Sachidanandam, R., and Collins, K. (2010). A growth-essential Tetrahymena Piwi protein carries tRNA fragment cargo. Genes & development *24*, 2742-2747.

Cozen, A.E., Quartley, E., Holmes, A.D., Hrabeta-Robinson, E., Phizicky, E.M., and Lowe, T.M. (2015). ARM-seq: AlkB-facilitated RNA methylation sequencing reveals a complex landscape of modified tRNA fragments. Nat Methods *12*, 879-884.

Crick, F.H. (1966). Codon--anticodon pairing: the wobble hypothesis. J Mol Biol *19*, 548-555.

Deng, J., Ptashkin, R.N., Chen, Y., Cheng, Z., Liu, G., Phan, T., Deng, X., Zhou, J., Lee, I., Lee, Y.S.*, et al.* (2015). Respiratory Syncytial Virus Utilizes a tRNA Fragment to Suppress Antiviral Responses Through a Novel Targeting Mechanism. Mol Ther *23*, 1622-1629.

Dittmar, K.A., Goodenbour, J.M., and Pan, T. (2006). Tissue-specific differences in human transfer RNA expression. PLoS Genet *2*, e221.

dos Reis, M., Savva, R., and Wernisch, L. (2004). Solving the riddle of codon usage preferences: a test for translational selection. Nucleic Acids Res *32*, 5036-5044.

Fu, H., Feng, J., Liu, Q., Sun, F., Tie, Y., Zhu, J., Xing, R., Sun, Z., and Zheng, X. (2009). Stress induces tRNA cleavage by angiogenin in mammalian cells. FEBS letters *583*, 437-442.

Gehrke, C.W., Kuo, K.C., Waalkes, T.P., and Borek, E. (1979). Patterns of urinary excretion of modified nucleosides. Cancer Res *39*, 1150-1153.

Geissler, R., Simkin, A., Floss, D., Patel, R., Fogarty, E.A., Scheller, J., and Grimson, A. (2016). A widespread sequence-specific mRNA decay pathway mediated by hnRNPs A1 and A2/B1. Genes & development *30*, 1070-1085.

Gingold, H., Tehler, D., Christoffersen, N.R., Nielsen, M.M., Asmar, F., Kooistra, S.M., Christophersen, N.S., Christensen, L.L., Borre, M., Sorensen, K.D.*, et al.* (2014). A dual program for translation regulation in cellular proliferation and differentiation. Cell *158*, 1281-1292.

Gogakos, T., Brown, M., Garzia, A., Meyer, C., Hafner, M., and Tuschl, T. (2017). Characterizing Expression and Processing of Precursor and Mature Human tRNAs by Hydro-tRNAseq and PAR-CLIP. Cell Rep *20*, 1463-1475.

Goncalves, K.A., Silberstein, L., Li, S., Severe, N., Hu, M.G., Yang, H., Scadden, D.T., and Hu, G.F. (2016). Angiogenin Promotes Hematopoietic Regeneration by Dichotomously Regulating Quiescence of Stem and Progenitor Cells. Cell *166*, 894-906.

Goodarzi, H., Elemento, O., and Tavazoie, S. (2009). Revealing global regulatory perturbations across human cancers. Mol Cell *36*, 900-911.

Goodarzi, H., Liu, X., Nguyen, H.C., Zhang, S., Fish, L., and Tavazoie, S.F. (2015). Endogenous tRNA-Derived Fragments Suppress Breast Cancer Progression via YBX1 Displacement. Cell *161*, 790-802.

Goodarzi, H., Nguyen, H.C.B., Zhang, S., Dill, B.D., Molina, H., and Tavazoie, S.F. (2016). Modulated Expression of Specific tRNAs Drives Gene Expression and Cancer Progression. Cell *165*, 1416-1427.

Gottlieb, E., and Steitz, J.A. (1989). Function of the mammalian La protein: evidence for its action in transcription termination by RNA polymerase III. EMBO J *8*, 851-861.

Guerrier-Takada, C., Gardiner, K., Marsh, T., Pace, N., and Altman, S. (1983). The RNA moiety of ribonuclease P is the catalytic subunit of the enzyme. Cell *35*, 849-857.

Gustafsson, C., Govindarajan, S., and Minshull, J. (2004). Codon bias and heterologous protein expression. Trends Biotechnol *22*, 346-353.

Hafner, M., Landthaler, M., Burger, L., Khorshid, M., Hausser, J., Berninger, P., Rothballer, A., Ascano, M., Jr., Jungkamp, A.C., Munschauer, M.*, et al.* (2010). Transcriptome-wide identification of RNA-binding protein and microRNA target sites by PAR-CLIP. Cell *141*, 129-141.

Hamilton, B.J., Burns, C.M., Nichols, R.C., and Rigby, W.F. (1997). Modulation of AUUUA response element binding by heterogeneous nuclear ribonucleoprotein A1 in human T lymphocytes. The roles of cytoplasmic location, transcription, and phosphorylation. The Journal of biological chemistry *272*, 28732-28741.

Haussecker, D., Huang, Y., Lau, A., Parameswaran, P., Fire, A.Z., and Kay, M.A. (2010). Human tRNA-derived small RNAs in the global regulation of RNA silencing. RNA *16*, 673-695.

Helm, M., Giege, R., and Florentz, C. (1999). A Watson-Crick base-pair-disrupting methyl group (m1A9) is sufficient for cloverleaf folding of human mitochondrial tRNALys. Biochemistry *38*, 13338-13346.

Honda, S., Loher, P., Shigematsu, M., Palazzo, J.P., Suzuki, R., Imoto, I., Rigoutsos, I., and Kirino, Y. (2015). Sex hormone-dependent tRNA halves enhance cell proliferation in breast and prostate cancers. Proc Natl Acad Sci U S A *112*, E3816-3825.

Huelga, S.C., Vu, A.Q., Arnold, J.D., Liang, T.Y., Liu, P.P., Yan, B.Y., Donohue, J.P., Shiue, L., Hoon, S., Brenner, S.*, et al.* (2012). Integrative genome-wide analysis reveals cooperative regulation of alternative splicing by hnRNP proteins. Cell Rep *1*, 167-178.

Ingolia, N.T., Ghaemmaghami, S., Newman, J.R., and Weissman, J.S. (2009). Genome-wide analysis in vivo of translation with nucleotide resolution using ribosome profiling. Science *324*, 218-223.

Ishimura, R., Nagy, G., Dotu, I., Zhou, H., Yang, X.L., Schimmel, P., Senju, S., Nishimura, Y., Chuang, J.H., and Ackerman, S.L. (2014). RNA function. Ribosome stalling induced by
mutation of a CNS-specific tRNA causes neurodegeneration. Science *345*, 455-459.

Jean-Philippe, J., Paz, S., and Caputi, M. (2013). hnRNP A1: the Swiss army knife of gene expression. Int J Mol Sci *14*, 18999-19024.

Kadaba, S., Krueger, A., Trice, T., Krecic, A.M., Hinnebusch, A.G., and Anderson, J. (2004). Nuclear surveillance and degradation of hypomodified initiator tRNAMet in S. cerevisiae. Genes & development *18*, 1227-1240.

Karaca, E., Weitzer, S., Pehlivan, D., Shiraishi, H., Gogakos, T., Hanada, T., Jhangiani, S.N., Wiszniewski, W., Withers, M., Campbell, I.M.*, et al.* (2014). Human CLP1 mutations alter tRNA biogenesis, affecting both peripheral and central nervous system function. Cell *157*, 636-650.

Kim, H.K., Fuchs, G., Wang, S., Wei, W., Zhang, Y., Park, H., Roy-Chaudhuri, B., Li, P., Xu, J., Chu, K.*, et al.* (2017). A transfer-RNA-derived small RNA regulates ribosome biogenesis. Nature *552*, 57-62.

Kirchner, S., and Ignatova, Z. (2015). Emerging roles of tRNA in adaptive translation, signalling dynamics and disease. Nat Rev Genet *16*, 98-112.

Konevega, A.L., Soboleva, N.G., Makhno, V.I., Semenkov, Y.P., Wintermeyer, W., Rodnina, M.V., and Katunin, V.I. (2004). Purine bases at position 37 of tRNA stabilize codon-anticodon interaction in the ribosomal A site by stacking and Mg2+-dependent interactions. RNA *10*, 90-101.

Kumar, P., Anaya, J., Mudunuri, S.B., and Dutta, A. (2014). Meta-analysis of tRNA derived RNA fragments reveals that they are evolutionarily conserved and associate with AGO proteins to recognize specific RNA targets. BMC Biol *12*, 78.

Ladner, J.E., Jack, A., Robertus, J.D., Brown, R.S., Rhodes, D., Clark, B.F., and Klug, A. (1975). Structure of yeast phenylalanine transfer RNA at 2.5 A resolution. Proc Natl Acad Sci U S A *72*, 4414-4418.

Lareau, L.F., Hite, D.H., Hogan, G.J., and Brown, P.O. (2014). Distinct stages of the translation elongation cycle revealed by sequencing ribosome-protected mRNA fragments. Elife *3*, e01257.

Lee, S.R., and Collins, K. (2005). Starvation-induced cleavage of the tRNA anticodon loop in Tetrahymena thermophila. The Journal of biological chemistry *280*, 42744-42749.

Lee, Y.S., Shibata, Y., Malhotra, A., and Dutta, A. (2009). A novel class of small RNAs: tRNA-derived RNA fragments (tRFs). Genes & development *23*, 2639-2649.

Licatalosi, D.D., Mele, A., Fak, J.J., Ule, J., Kayikci, M., Chi, S.W., Clark, T.A., Schweitzer, A.C., Blume, J.E., Wang, X.*, et al.* (2008). HITS-CLIP yields genome-wide insights into brain alternative RNA processing. Nature *456*, 464-469.

Maraia, R.J., Kenan, D.J., and Keene, J.D. (1994). Eukaryotic transcription termination factor La mediates transcript release and facilitates reinitiation by RNA polymerase III. Mol Cell Biol *14*, 2147-2158.

Maraia, R.J., and Lamichhane, T.N. (2011). 3' processing of eukaryotic precursor tRNAs. Wiley interdisciplinary reviews RNA *2*, 362-375.

Maraia, R.J., Mattijssen, S., Cruz-Gallardo, I., and Conte, M.R. (2017). The La and related RNA-binding proteins (LARPs): structures, functions, and evolving perspectives. Wiley interdisciplinary reviews RNA *8*.

Martindale, J.L., and Holbrook, N.J. (2002). Cellular response to oxidative stress: signaling for suicide and survival. J Cell Physiol *192*, 1-15.

Mattijssen, S., Arimbasseri, A.G., Iben, J.R., Gaidamakov, S., Lee, J., Hafner, M., and Maraia, R.J. (2017). LARP4 mRNA codon-tRNA match contributes to LARP4 activity for ribosomal protein mRNA poly(A) tail length protection. Elife *6*.

Maute, R.L., Schneider, C., Sumazin, P., Holmes, A., Califano, A., Basso, K., and Dalla-Favera, R. (2013). tRNA-derived microRNA modulates proliferation and the DNA damage response and is down-regulated in B cell lymphoma. Proc Natl Acad Sci U S A *110*, 1404-1409.

McGlincy, N.J., and Ingolia, N.T. (2017). Transcriptome-wide measurement of translation by ribosome profiling. Methods *126*, 112-129.

Mili, S., and Steitz, J.A. (2004). Evidence for reassociation of RNA-binding proteins after cell lysis: implications for the interpretation of immunoprecipitation analyses. RNA *10*, 1692-1694.

Munz, M., Baeuerle, P.A., and Gires, O. (2009). The emerging role of EpCAM in cancer and stem cell signaling. Cancer Res *69*, 5627-5629.

Nicassio, F., Corrado, N., Vissers, J.H., Areces, L.B., Bergink, S., Marteijn, J.A., Geverts, B., Houtsmuller, A.B., Vermeulen, W., Di Fiore, P.P.*, et al.* (2007). Human USP3 is a chromatin modifier required for S phase progression and genome stability. Curr Biol *17*, 1972-1977.
Pan, T. (2018). Modifications and functional genomics of human transfer RNA. Cell Res *28*, 395-404.

Parisien, M., Wang, X., and Pan, T. (2013). Diversity of human tRNA genes from the 1000-genomes project. RNA biology *10*, 1853-1867.

Paton, C.M., and Ntambi, J.M. (2009). Biochemical and physiological function of stearoyl-CoA desaturase. Am J Physiol Endocrinol Metab *297*, E28-37.

Paushkin, S.V., Patel, M., Furia, B.S., Peltz, S.W., and Trotta, C.R. (2004). Identification of a human endonuclease complex reveals a link between tRNA splicing and pre-mRNA 3' end formation. Cell *117*, 311-321.

Pavon-Eternod, M., Gomes, S., Geslain, R., Dai, Q., Rosner, M.R., and Pan, T. (2009). tRNA over-expression in breast cancer and functional consequences. Nucleic Acids Res *37*, 7268-7280.

Peebles, C.L., Ogden, R.C., Knapp, G., and Abelson, J. (1979). Splicing of yeast tRNA precursors: a two-stage reaction. Cell *18*, 27-35.

Pershing, N.L., Lampson, B.L., Belsky, J.A., Kaltenbrun, E., MacAlpine, D.M., and Counter, C.M. (2015). Rare codons capacitate Kras-driven de novo tumorigenesis. J Clin Invest *125*, 222-233.

Phizicky, E.M., and Hopper, A.K. (2010). tRNA biology charges to the front. Genes & development *24*, 1832-1860.

Presnyak, V., Alhusaini, N., Chen, Y.H., Martin, S., Morris, N., Kline, N., Olson, S., Weinberg, D., Baker, K.E., Graveley, B.R.*, et al.* (2015). Codon optimality is a major determinant of mRNA stability. Cell *160*, 1111-1124.

Quigley, G.J., and Rich, A. (1976). Structural domains of transfer RNA molecules. Science *194*, 796-806.

Radhakrishnan, A., Chen, Y.H., Martin, S., Alhusaini, N., Green, R., and Coller, J. (2016). The DEAD-Box Protein Dhh1p Couples mRNA Decay and Translation by Monitoring Codon Optimality. Cell *167*, 122-132 e129.

Saikia, M., Krokowski, D., Guan, B.J., Ivanov, P., Parisien, M., Hu, G.F., Anderson, P., Pan, T., and Hatzoglou, M. (2012). Genome-wide identification and quantitative analysis of cleaved tRNA fragments induced by cellular stress. The Journal of biological chemistry *287*, 42708-42725.

Schaffer, A.E., Eggens, V.R., Caglayan, A.O., Reuter, M.S., Scott, E., Coufal, N.G., Silhavy, J.L., Xue, Y., Kayserili, H., Yasuno, K.*, et al.* (2014). CLP1 founder mutation links tRNA splicing and maturation to cerebellar development and neurodegeneration. Cell *157*, 651-663.

Schimmel, P. (2018). The emerging complexity of the tRNA world: mammalian tRNAs beyond protein synthesis. Nat Rev Mol Cell Biol *19*, 45-58.

Shah, A., Qian, Y., Weyn-Vanhentenryck, S.M., and Zhang, C. (2017). CLIP Tool Kit (CTK): a flexible and robust pipeline to analyze CLIP sequencing data. Bioinformatics *33*, 566-567.

Sharma, U., Conine, C.C., Shea, J.M., Boskovic, A., Derr, A.G., Bing, X.Y., Belleannee, C., Kucukural, A., Serra, R.W., Sun, F.*, et al.* (2016). Biogenesis and function of tRNA fragments during sperm maturation and fertilization in mammals. Science *351*, 391-396.

The Gene Ontology, C. (2017). Expansion of the Gene Ontology knowledgebase and resources. Nucleic Acids Res *45*, D331-D338.

Thompson, D.M., Lu, C., Green, P.J., and Parker, R. (2008). tRNA cleavage is a conserved response to oxidative stress in eukaryotes. RNA *14*, 2095-2103.

Thompson, D.M., and Parker, R. (2009a). The RNase Rny1p cleaves tRNAs and promotes cell death during oxidative stress in Saccharomyces cerevisiae. J Cell Biol *185*, 43-50.

Thompson, D.M., and Parker, R. (2009b). Stressing out over tRNA cleavage. Cell *138*, 215-219.

Torrent, M., Chalancon, G., de Groot, N.S., Wuster, A., and Madan Babu, M. (2018). Cells alter their tRNA abundance to selectively regulate protein synthesis during stress conditions. Sci Signal *11*.

Truitt, M.L., and Ruggero, D. (2016). New frontiers in translational control of the cancer genome. Nat Rev Cancer *16*, 288-304.

Ule, J., Jensen, K.B., Ruggiu, M., Mele, A., Ule, A., and Darnell, R.B. (2003). CLIP identifies Nova-regulated RNA networks in the brain. Science *302*, 1212-1215.

Weitzer, S., and Martinez, J. (2007). The human RNA kinase hClp1 is active on 3' transfer RNA exons and short interfering RNAs. Nature *447*, 222-226.

Wohlgemuth, S.E., Gorochowski, T.E., and Roubos, J.A. (2013). Translational sensitivity of the Escherichia coli genome to fluctuating tRNA availability. Nucleic Acids Res *41*, 8021-8033.

Wolin, S.L., and Cedervall, T. (2002). The La protein. Annu Rev Biochem *71*, 375-403.

Wu, C.C., Zinshteyn, B., Wehner, K.A., and Green, R. (2019). High-Resolution Ribosome Profiling Defines Discrete Ribosome Elongation States and Translational Regulation during Cellular Stress. Mol Cell *73*, 959-970 e955.

Xiao, Z., Zou, Q., Liu, Y., and Yang, X. (2016). Genome-wide assessment of differential translations with ribosome profiling data. Nat Commun *7*, 11194.

Yamasaki, S., Ivanov, P., Hu, G.F., and Anderson, P. (2009). Angiogenin cleaves tRNA and promotes stress-induced translational repression. J Cell Biol *185*, 35-42.

Yoo, C.J., and Wolin, S.L. (1997). The yeast La protein is required for the 3' endonucleolytic cleavage that matures tRNA precursors. Cell *89*, 393-402.

Zheng, G., Qin, Y., Clark, W.C., Dai, Q., Yi, C., He, C., Lambowitz, A.M., and Pan, T. (2015). Efficient and quantitative high-throughput tRNA sequencing. Nat Methods *12*, 835-837.

Zhong, J., Xiao, C., Gu, W., Du, G., Sun, X., He, Q.Y., and Zhang, G. (2015). Transfer RNAs Mediate the Rapid Adaptation of Escherichia coli to Oxidative Stress. PLoS Genet *11*, e1005302.

Zhou, J., Liu, S., Chen, Y., Fu, Y., Silver, A.J., Hill, M.S., Lee, I., Lee, Y.S., and Bao, X. (2017). Identification of two novel functional tRNA-derived fragments induced in response to respiratory syncytial virus infection. J Gen Virol *98*, 1600-1610.